Zhang *et al. Chem Synth* 2023;3:28
DOI: 10.20517/cs.2023.17

Chemical Synthesis

Review

Open Access

Nanostructured intermetallics: from rational synthesis to energy electrocatalysis

Mingcheng Zhang[1], Qianqian Liu[1,2], Weipei Sun[1], Ke Sun[1], Yucheng Shen[1], Wei An[1], Lu Zhang[1], Hui Chen[1,*], Xiaoxin Zou[1,*]

[1]State Key Laboratory of Inorganic Synthesis and Preparative Chemistry, College of Chemistry, Jilin University, Changchun 130012, Jilin, China.
[2]School of Materials Science and Engineering, Xi'an University of Science and Technology, Xi'an 710054, Shannxi, China.

[*]**Correspondence to:** Prof. Xiaoxin Zou, State Key Laboratory of Inorganic Synthesis and Preparative Chemistry, College of Chemistry, Jilin University, 2699 Qianjin Street, Changchun 130012, Jilin, China. E-mail: xxzou@jlu.edu.cn; Prof. Hui Chen, State Key Laboratory of Inorganic Synthesis and Preparative Chemistry, College of Chemistry, Jilin University, 2699 Qianjin Street, Changchun 130012, Jilin, China. E-mail: chenhui@jlu.edu.cn

How to cite this article: Zhang M, Liu Q, Sun W, Sun K, Shen Y, An W, Zhang L, Chen H, Zou X. Nanostructured intermetallics: from rational synthesis to energy electrocatalysis. *Chem Synth* 2023;3:28. https://dx.doi.org/10.20517/cs.2023.17

Received: 20 Mar 2023 **First Decision:** 13 Apr 2023 **Revised:** 18 Apr 2023 **Accepted:** 26 Apr 2023 **Published:** 5 Jun 2023

Academic Editor: Bao-Lian Su **Copy Editor:** Dong-Li Li **Production Editor:** Dong-Li Li

Abstract

Intermetallics are a large family of structurally ordered alloys that combines a metal element with other metal/metalloid elements with a clearly defined stoichiometric ratio. Intermetallics possess abundant crystal structures and atomic packing motifs, giving rise to a great variety of electronic configurations and surface adsorption properties. The wide electronic and geometric diversity makes intermetallics a highly promising population for discovering advanced materials for various catalytic applications. This review presents recent advances in the reaction synthesis of intermetallic materials at the nanoscale and their energy-related electrocatalytic applications. Initially, we introduce general principles for the formation of stable intermetallic structures. Subsequently, we elaborate on common synthetic strategies of nanostructured intermetallics, such as thermal annealing, wet-chemical methods, metallothermic reduction, and template-directed synthesis. Furthermore, we discuss the wide employment of these intermetallic nanocatalysts in many different kinds of electrocatalytic applications, as well as highlight the theoretical and experimental evidence for establishing a reasonable relationship between atomic arrangement and catalytic activity. Finally, we propose some perspectives for future developments of intermetallic preparation and catalytic applications.

Keywords: Intermetallics, ordered arrangement, Hume-Rothery rule, electrocatalysis, energy conversion

INTRODUCTION

The chemical industry largely depends on heterogeneous catalysis, in which various metal materials are employed as attractive catalysts for the production of bulk chemicals, pharmaceuticals and agrochemicals[1-4]. For a given catalytic application, the catalysts should fulfill multiple criteria such as high activity, low cost, good selectivity and stability, which usually cannot be achieved by a single metal. Introducing another metal/metalloid component to form an alloy has long been used to drastically expand the property landscape and potentially meet these essential criteria[5,6]. The metallic alloys are typically separated into disordered structure (i.e., substitutional alloy) and ordered structure (i.e., intermetallic compound)[7,8]. While the substitutional alloy shows the crystal phase of one of constituting elements with varying composition and random atomic arrangement, the constituting elements in the intermetallic compounds have well-defined stoichiometry and highly ordered arrangement. At present, more than 25,000 intermetallic compounds are known since this concept was proposed by British metallurgists in 1914 [Figure 1]. These intermetallics possess complex crystal structures and unique chemical bonding, which are not easily obtained in random alloys and other compounds, providing novel patterns of electronic structures and great potential to discover new chemical properties, such as catalytic properties.

Early in the 1930s, the catalytic properties of intermetallics were investigated[9]. Among pioneering examples, Brown *et al.* reported intermetallic Tl_2Pb and Cd_3Cu_2 with good catalytic activities toward vapor-phase reduction of nitrobenzene[9,10]. The electrocatalytic application of intermetallic compounds started already back in the 1970s, when the development of fuel cell technology drove the great requirement for new electrocatalysts[11-13]. Some Pt and Ni-based intermetallics (e.g., PtPd, Ti_2Ni) were thus explored as potential fuel cell electrodes. Subsequently, the applications of intermetallic compounds expand to many electrocatalytic reactions such as water electrolysis, CO_2 reduction, and nitrogen fixation[14-19]. The alloy catalysts with intermetallic structures present great success in achieving high activity, because strong chemical interactions between the alloying elements modify the electronic structure and surface chemisorption properties. The peculiar crystal structure and chemical bonding in some intermetallics produce the unexpected catalytic benefits previously rooted. In many cases, the intermetallic alloy catalysts possess more superior catalytic and structural stability than their disordered counterparts, and benefit from the ordered arrangement and strong interactions of involved metals/metalloids to restrain segregation or decomposition during catalytic reactions[20,21].

The catalytic performances of intermetallics depend on their composition, crystal phase, shape, and size. Conventionally, intermetallic compounds are prepared by solid-state methods under high temperature and pressure conditions, leading to uncontrollable morphology and large particle size, which limit the catalytic exploitation of intermetallic structures[22,23]. It is only in the last twenty years that the great progress in modern synthetic chemistry promotes the wide catalytic applications of intermetallics, especially in the energy-relevant electrocatalytic fields. The new synthetic strategies and design principles can control the growth of nanoparticulate intermetallic materials to yield different crystal phases, shapes and sizes[24-28]. Moreover, the developments of advanced characterization tools and computational chemistry enable the opportunity to reveal the geometric and electronic effects that determine catalytic performance by using the intermetallic materials with homogeneous surface chemical environments as model catalysts[29-31]. It is important to offer an overview of the latest progress in chemical syntheses of shape-/size-/composition-controlled intermetallics and their electrocatalytic applications.

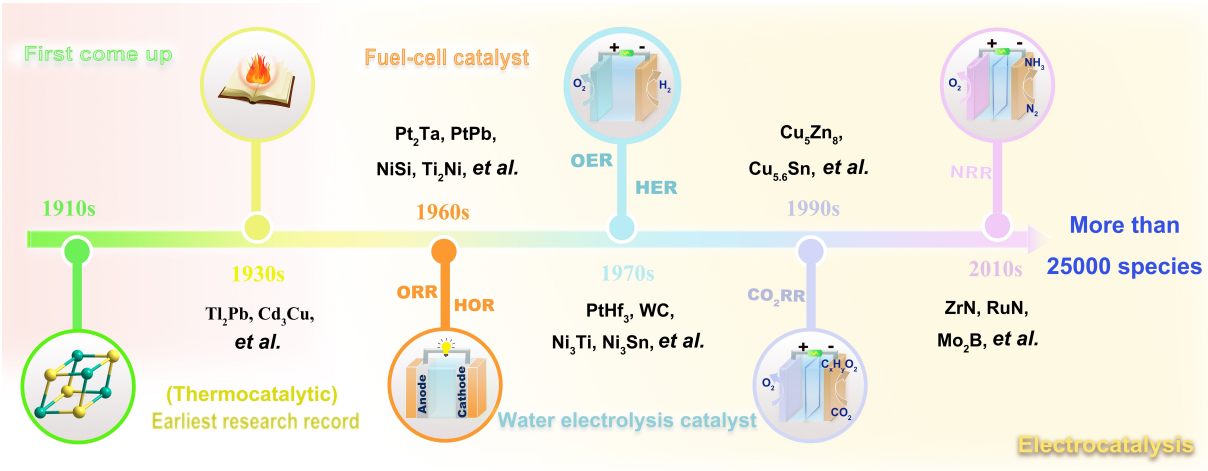

Figure 1. Development timeline infographic of intermetallic catalysts.

In this work, the recent research advances made in the synthesis of various intermetallics for important electrocatalytic reactions are reviewed. The basic principles of the formation of stable intermetallic structures are introduced, with emphasis on Hume-Rothery rules, phase diagrams, kinetics and thermodynamic analyses. Then, mainstream strategies to obtain nanostructured intermetallic materials and control the composition, crystal phase, shape, and size are outlined. In the next section, the representative use of intermetallic nanocrystals as electrocatalysts is discussed for various reactions including the hydrogen evolution reaction (HER), the oxygen reduction reaction (ORR), the CO_2 reduction reaction (CO_2RR) and the nitrogen reduction reaction (NRR). The role of these intermetallic structures in the electrochemical reactions is highlighted, and several perspectives on future investigations of intermetallic catalysts are proposed.

GENERAL PRINCIPLES FOR INTERMETALLIC FORMATION

Hume-rothery rules

Even the simplest bimetallic systems can be complex due to their different states of the intermediate phase, which include immiscible mixtures and miscible systems. Miscible systems can be further classified into random alloys, in which the atomic positions of the metals are disordered, and intermetallic alloys, in which the atomic positions are ordered. In the 1920s and 1930s, British metallurgist William Hume-Rothery and his colleagues proposed the Hume-Rothery Rules, which is an empirical guideline for determining the intermediate phase state of binary alloy systems[32,33]. This rule is based on factors such as atomic radius, crystal structure, electronegativity, and electronic structure, and can be a useful tool for designing binary alloys.

According to the Hume-Rothery Rules, when the atomic radii of two elements differ by more than 15%, they are difficult to miscible. For example, atomic radii of Co and Ag are 135 pm and 160 pm, respectively. Regardless of the ratio or temperature of the two metals, it is not possible to obtain a miscible system. Instead, an immiscible solid mixture will form [Figure 2A]. In contrast, Ni (135 pm) has a similar atomic radius to Co, and Ni-Co can form a miscible disordered alloy [Figure 2B]. In addition to atomic radius, the electronegativity difference ($\Delta\chi$) between the two metals also plays an important role in the formation of intermetallic compounds. A large electronegativity difference strengthens the chemical bond between the two metals, making it more thermodynamically inclined to generate an ordered structure. For example, Ni and Co have similar electronegativities (χ_{Ni} = 1.92 and χ_{Co} = 1.88), but Pd has a higher electronegativity of 2.2.

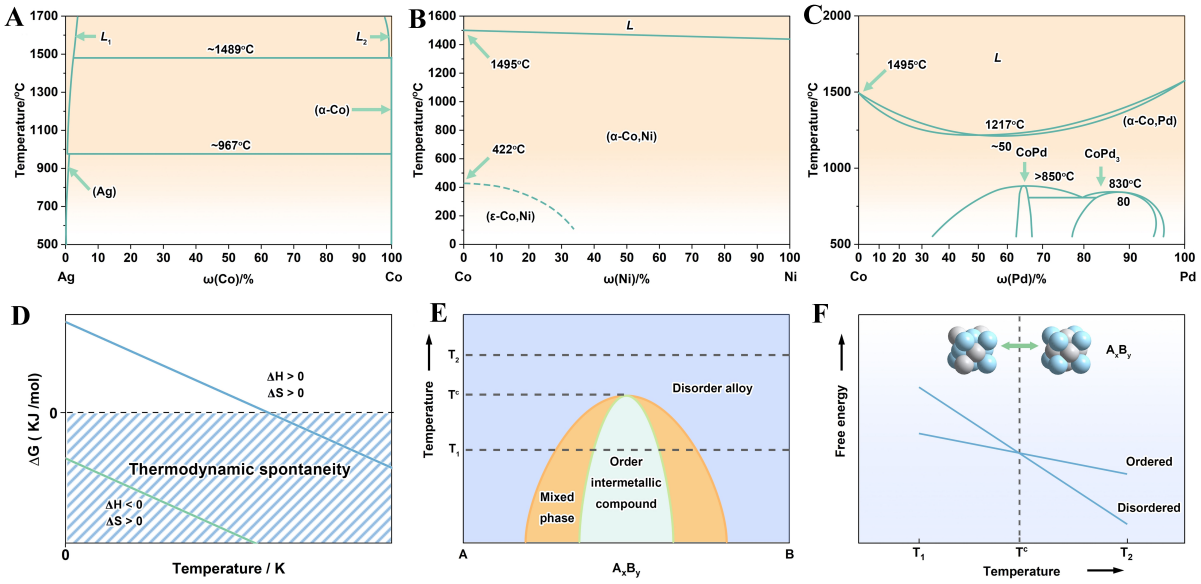

Figure 2. (A-C) Phase diagrams of three binary alloy systems. (A) Co-Ag immiscible system; (B) Co-Ni disordered alloy system; (C) Co-Pd ordered intermetallic compound system; (D) Schematic of the influence of different enthalpy and entropy on Gibbs free energy; (E) Phase diagram and critical transition temperature of typical ordered intermetallic compounds; (F) Comparison of free energies between disordered alloys and ordered intermetallic compounds under A_xB_y stoichiometry in different temperatures.

Pd and Co can form both random solid solutions and ordered intermetallic compounds, such as Pd_3Co and PdCo, under specific conditions [Figure 2C].

When Cu family elements form alloys with polyvalent metal elements (such as Zn, Ga, and Ge), the atomic radius and electronegativity difference become secondary factors, and the electron concentration effects become dominant[34]. The specific phases can be predicted by the average number of itinerant electrons per atom (**e/a**), as shown in a corresponding between phase and **e/a** relationship in Figure 3. In other words, the maximum solubility of the solute element will decrease as the **e/a** increases to ensure that the **e/a** of alloy is at a specific value. For example, when Zn, Ga and Ge form α-phase alloys with Cu, respectively, the maximum solubility is 38%, 20% and 12%. The **e/a** of $Zn_{0.38}Cu_{0.62}$ is easily calculated to be 1.38, and the **e/a** of the remaining two systems is also about 1.4. Different from the first two empirical rules, the Hume-Rothery electron concentration effect rule has been further explained with the development of condensed matter physics. In 1936, Mott and Jones successfully explained this rule by using the nearly free-electron model in the first Brillouin region[35]. According to this model, the critical **e/a** [$(\mathbf{e/a})_c$] of the system can be given by the spheroidal electron cloud tangent to the first Brillouin region [Figure 3]. For example, the $(\mathbf{e/a})_c$ values of α-, β- and γ-phase are 1.362, 1.480 and 1.538, which are basically consistent with the experimental results. The electron concentration effect is still widely studied today, for example, by using the total number of electrons as a new descriptor, and by trying to extend the rule to other transition metals.

The Hume-Rothery rules are effective for determining the crystal structures of numerous intermetallic compounds. However, these rules have limitations and are not applicable to all binary systems. For instance, the 18-n rule can be employed to ascertain the bond formation of intermetallic compounds composed of transition metals and *p*-block elements[36,37]. Meanwhile, the Zintl phase, which is formed by alkali/alkaline earth metals and *p*-block elements, does not adhere to the Hume-Rothery rules. A typical example is NaTl, which exhibits properties of brittleness, diamagnetism, and low conductivity despite being comprised of two metals. These nonmetallic properties arise from the significant electronegativity difference between sodium

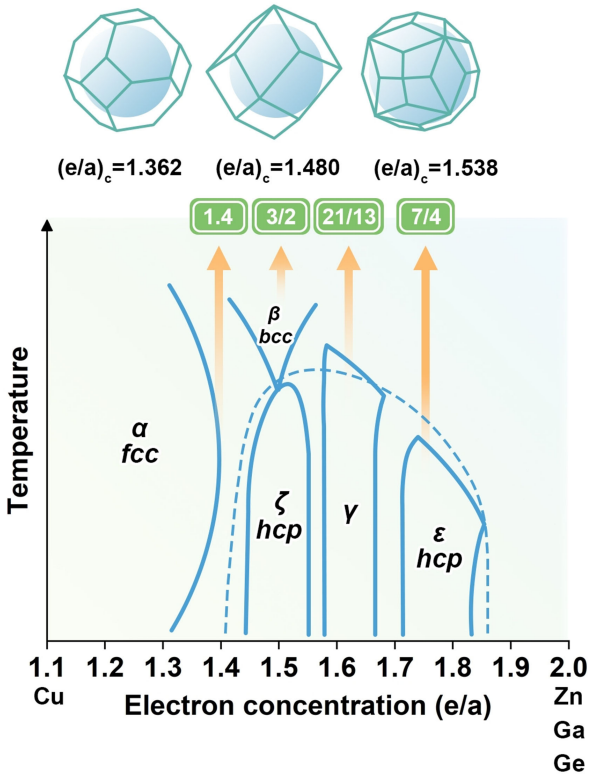

Figure 3. Schematic of the relationship between electron concentration (**e/a**) and crystal phase structure, and the First Brillouin Zone and critical electron concentration $(e/a)_c$ values of typical crystal phase structures (α-, β- and γ-phase).

and thallium. After thallium accepts an electron from sodium, it still fails to achieve an octet (only four electrons), resulting in the formation of a regular tetrahedral network similar to carbon atoms in diamonds. This is so-called the Zintl-Klemm counting scheme[38-40], in which the anion of the Zintl phase forms polyanionic substructures resembling elements with the same number of outermost electrons, such as white phosphorus (tetrahedral P_4) and sulfur (circular S_8). However, these compounds are infrequently utilized as electrocatalysts due to their poor electrical conductivity, and thus will not be elaborated upon in this review.

Thermodynamic analysis and phase diagram

The Hume-Rothery rules is an empirical guideline used to predict the conditions under which metallic alloys will exhibit miscibility. The Gibbs free energy of mixing is a key determinant in judging whether the system can spontaneously become miscible. We also take the binary system as a simple example, and the Gibbs free energy change in the mixing process (ΔG_{bulk}) of the bulk system can be written as follows.

$$\Delta G_{bulk} = \Delta H - \mathrm{T_{bulk}}\Delta S \quad (1)$$

where ΔH is the enthalpy change of mixing, T is the absolute temperature, and ΔS is the entropy change of mixing. It is well established that the entropy of the system must increase during the mixing process, meaning that ΔS is always positive. The sign of ΔH depends on whether the formation of new bonds in the system is exothermic or endothermic. If the ΔH is negative, then the ΔG will be less than zero at any

temperature leading to a miscible system, such as the Co-Ni system. However, when ΔH is positive, the effect of temperature should be considered [Figure 2D]. The influence of $T\Delta S$ on the Gibbs free energy of the system is relatively small at lower temperatures, which is because the enthalpy change is generally 2-3 orders of magnitude larger than the entropy change. For example, in the Co-Ag immiscible system, the ΔH is considerably larger than zero, so the two metals are still not miscible at 2000 K. This formula can also be used to guide the transition process between disordered alloys and ordered intermetallic compounds. When $\Delta G = 0$, the system is in a two-phase mixed equilibrium state, and the temperature is called critical phase-transition temperature (T^c)[7]. In general, the enthalpy change of the disorder-to-order transition is negative, as intermetallic compounds typically have higher bond energies, making the ordered system more thermodynamically stable. The entropy change of this process is also negative, as the atoms in the system become more ordered. Thus, low temperatures favor the formation of ordered metal compounds, while high temperatures favor the formation of disordered alloys [Figure 2E and F].

In practical systems, it is critical to take into account the effect of surface energy, which is not present in ideal bulk systems. The smaller the particle size, the larger the influence of surface energy on the overall energy. As a result, the equation for Gibbs free energy change in the mixing process needs to be modified to consider surface energy[41,42]:

$$\Delta G_{nano} = \Delta H - \mathrm{T_{nano}}\Delta S + \mathrm{A}\Delta\gamma \quad (2)$$

where A is the surface area of the particle and $\Delta\gamma$ is the change in surface energy. When bulk system and nanoparticle system reach critical phase-transition temperature, ΔG_{bulk} and ΔG_{nano} are zero. Combined with equations 1 and 2, the T^c of the two systems can be written as equation 3[28].

$$\frac{\mathrm{T^c_{nano}}}{\mathrm{T^c_{bulk}}} = 1 + \frac{\mathrm{A}}{\mathrm{V}} \times \frac{\Delta\gamma}{\Delta H_v} \quad (3)$$

where ΔH_v is volume-specific bulk enthalpy. In the disorder-to-order transition, it is clear that ΔH_v is negative, the same sign as ΔH. And since the average bond energy is higher on ordered surfaces, $\Delta\gamma$ is also negative. According to equation 3, as the particle size of nanoparticles decreases, the specific surface area (A/V) increases. The nanoparticle system should have a lower critical phase-transition temperature than the bulk system[43,44]. A typical example of this conclusion is the discovery by Alloyeau *et al.* that CoPt nanoparticles have a T^c of 175-325 ℃ lower than bulk materials[45]. Moreover, the exposed surface of the nanoparticles also influences the energy of the system, as the surface energy of different crystal faces can vary. In conclusion, the Gibbs free energy and the critical phase transition temperature of the system will be impacted by the composition, particle size, shape, and other factors.

Although thermodynamics at a given temperature can provide an accurate indication of whether a system is miscible at a given temperature, it is still not intuitive. The phase diagram can visualize the state of the reaction system and provide a preliminary reference for the stoichiometric ratio and temperature required for the synthesis of metal compounds. The Gibbs phase rule is the basis for phase diagrams, a formula introduced by Josiah Willard Gibbs in the 1870s[46]. This rule holds that the state of a system is entirely

described by its thermodynamic parameters (e.g., temperature and pressure) at equilibrium.

$$F = C - P + 2 \quad (4)$$

where C is the composition fraction of the system, P is the number of phases, and F is the number of degrees of freedom, that is, the number of independent variations of the system. For a binary system with C = 2, the number of degrees of freedom is given by F = 4 - P. If only one phase is present in the system (P = 1), then F is three, meaning that the system's pressure, temperature, and composition can vary independently.

H. W. Bakhuis Roozeboom applied this rule and produced the first iron-carbon phase diagram in 1900[47]. The phase diagram can intuitively show the equilibrium state of the system at any temperature. Additionally, the phase diagram can be used to predict the behavior of the high-temperature system during cooling. Moreover, intermetallic compounds with fixed composition are represented as narrow regions or vertical lines in the phase diagram. This can make it challenging to experimentally plot phase diagrams. By combining theoretical simulation and thermodynamic analysis, phase diagrams can be accurately mapped and the prediction of new intermetallic compounds becomes possible. The thermodynamic parameter, pressure, which is more difficult to control in experiments, can also be easily obtained from computational simulations. For example, Clarke *et al.* utilized DFT calculations to create the temperature-pressure phase diagram of the Cu-Bi binary system and successfully synthesized superconducting $Cu_{11}Bi_7$[48]. Theoretical prediction combined with high-throughput screening and machine learning methods has played an important role in predicting and characterizing the properties of intermetallic compounds[49,50].

Kinetics analysis

Thermodynamics and phase diagram can provide crucial guidance for the synthesis of metallic compounds, but a range of kinetic factors need to be considered in the actual reaction process. While thermodynamic conditions may be favorable during synthesis, the presence of kinetic energy barriers can result in the formation of metastable structures. In fact, the successful preparation of ordered intermetallic compounds is dependent on balancing the thermodynamic driving force and the kinetic energy barrier, and the system must cross the activation energy barrier to reach the most stable thermodynamic state[51] [Figure 4A].

The Johnson-Mehl-Avrami-Kolmogorov (JMAK) theory describes in detail the dynamics during the formation of ordered phases[52-54]. Here we will examine the two fundamental processes in the transformation from disorder to order, the formation of new phases (nucleation) and the rearrangement of local atoms (diffusion). According to the Arrhenius equation, the reaction rates of the two processes are as follows.

$$k_1 = A_1 e^{-\frac{\Delta G}{k_B T}} \quad (5)$$

$$k_2 = A_2 e^{-\frac{E_a}{k_B T}} \quad (6)$$

where A_1 and A_2 are the respective preexponential factors, k_B is the Boltzmann constant, ΔG is the Gibbs free energy change in phase transition, E_a is the activation energy of atomic diffusion, and T is the absolute temperature. For the reaction to occur, ΔG must be negative, while the remaining parameters (A_1, A_2, k_B, E_a, and T) are all positive. Therefore, k_1 and k_2 have diametrically opposite tendencies with respect to temperature. The reaction rate of k_1 decreases while that of k_2 increases with increasing temperature. The overall transition rate depends on the product of k_1 and k_2, so there exists an optimal transition temperature. In other words, the curve of the total rate as a function of temperature [Figure 4B] shows a volcanic pattern[55,56].

Particle size also influences the dynamics of the "disorder-to-order" process. Smaller particles will reduce the thermodynamic driving force and thus cause a decrease in k_1, as described in Equation 2. However, diffusion is easier in small particles. Therefore, there may also be an optimal range of particle sizes that is most favorable for the formation of ordered intermetallic compounds. In addition, the hole concentration and the interatomic bond strength also influence the reaction rate. Generally speaking, increasing the concentration of vacancies effectively facilitates the phase transition process because the activation energy of vacancy diffusion is lower[57]. In summary, several factors including temperature, composition, particle size and shape, and hole concentration must be considered to balance the thermodynamic driving force and kinetic energy barrier during the synthesis of ordered intermetallic compounds[58-63].

SYNTHESIS OF INTERMETALLICS

This section mainly introduces some main methods for the synthesis of nanoscale intermetallic compounds, although there are some traditional methods, such as solid-state synthesis[64,65], arc melting[66,67], and high-energy ball milling[68,69], which are widely used to synthesize intermetallic compounds. However, these synthetic methods usually have uncontrollable crystallization process, large grain size, and easy-to-generate miscible phase. Therefore, these methods are not summarized in this review. In the following, we summarize several important strategies for nanoscale intermetallic compound synthesis.

Thermal annealing

Thermal annealing, which heats random alloys at high temperatures for a sufficiently long time, is the simplest and most straightforward way to generate intermetallic compounds [Figure 5A]. According to thermodynamic and kinetic analyses, random alloy structures are more easily generated than intermetallic compounds when the reaction temperature is maintained below the disordered-to-ordered transition temperature. At elevated temperatures, thermal vibration of metal atoms is promoted, facilitating the diffusion of the metal and making it easier for random alloys to cross the barrier to form ordered compounds[7,28]. Using this method, a variety of bimetallic and trimetallic compounds, as well as intermetallic semiconductors and superconducting nanocrystals, have been synthesized. However, the

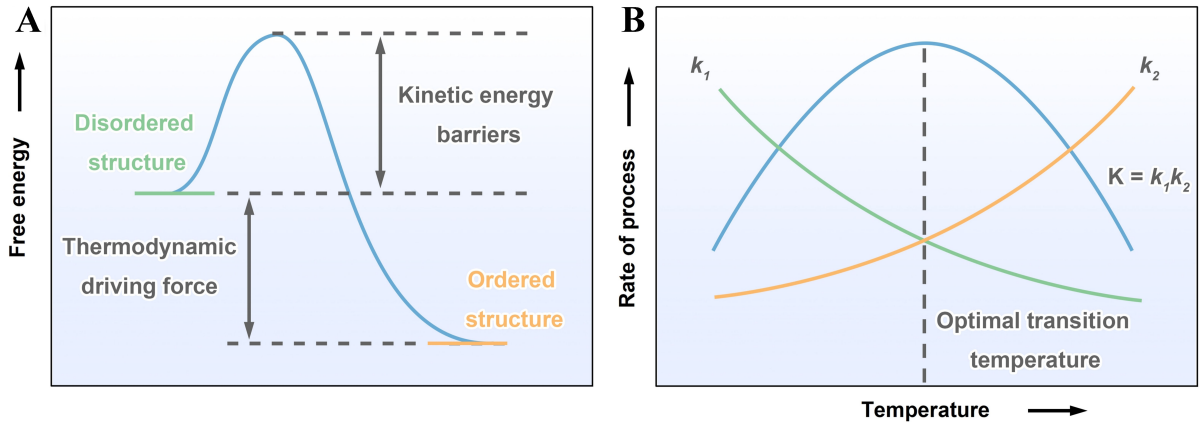

Figure 4. (A) Schematic of the free energy of the disordered structure converted to the ordered structure; (B) Schematic of nucleation rate, diffusion rate and total reaction rate as a function of temperature.

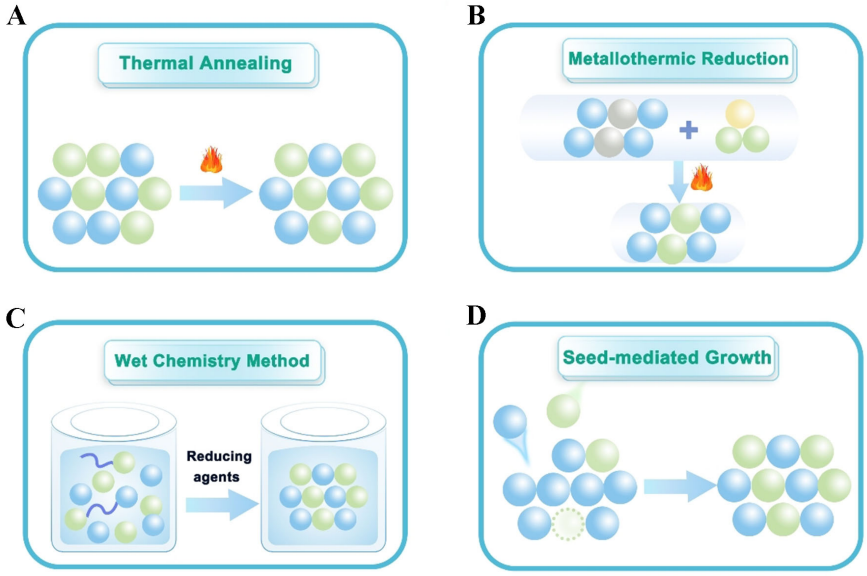

Figure 5. Schematic of the main synthesis methods for intermetallic compounds, including (A) thermal annealing; (B) metallothermic reduction; (C) wet chemistry method; and (D) seed-mediated growth.

thermal annealing method also has its disadvantages: higher annealing temperature will promote Ostwald ripening and aggregation, which results in the increase of nanocrystal size and uneven size distribution[70]. At the same time, the catalytic performance of intermetallic compound nanocrystals is reduced. Therefore, it is necessary to control the annealing temperature and annealing time, and to select appropriate support and coating layers to prevent aggregation of nanocrystals at high temperatures.

Direct annealing is currently the most widely used method to generate ordered intermetallic nanocrystals. In this process, random alloys obtained by the liquid phase method were used as primary intermediates, and then they were converted into atomically ordered intermetallic nanocrystals by heat treatment in an atmosphere or vacuum. Due to the relatively high kinetic barriers involved in atomic ordering, annealing at high temperatures (usually > 500 °C) and/or long times is required. For example, Abe *et al.* converted

atomically disordered Pt_3Ti nanoparticles into larger atomically ordered Pt_3Ti nanoparticles by annealing above 500 °C[71]. The authors annealed Pt_3Ti in vacuum at various temperatures and analyzed the PXRD profiles of the products, and they found that when the annealing temperature exceeds 550 °C, the PXRD of the annealed product shows the superlattice peak of Pt_3Ti in the ordered Cu_3Au-type structure. When the annealing temperature was further increased to 600 °C, the intensity of the above lattice peaks was improved. The results indicate that the annealing temperature is an important parameter in adjusting the order degree of the prepared nanocrystals. However, higher annealing temperatures inevitably lead to a sharp increase in particle size. Atomically disordered Pt_3Ti nanoparticles with a particle size of 3 ± 0.4 nm were annealed in vacuum at 600 °C and ordered Pt_3Ti nanoparticles with a particle size of 37 ± 23 nm were obtained. Chi *et al.* synthesized a series of Pt_3Co nanocrystals with different atomic arrangements during *in situ* annealing and observed five distinct stages of element rearrangement on the surface of nanocrystals by scanning transmission electron microscopy[72]. They found that when the sample temperature was raised to 600 °C and held for 20 min, the ordered Pt_3Co phase began to nucleate on {001}. By prolonging the annealing time at the same temperature, it is advantageous to form fully ordered phases with similar morphology. Therefore, careful selection of annealing temperature, annealing time, and annealing atmosphere plays a crucial role in promoting the degree of order, size, and shape of the final product.

Support-assisted annealing. Unlike direct annealing, the support-assisted annealing method deposits nanocrystals on stable supports with a larger surface area. The catalyst support can prevent unwanted aggregation of the active catalyst during thermal annealing[73]. In addition, electron rearrangement occurs at the interface between nanocrystals and support, which can increase the electron density of nanocrystals and improve the performance of catalysts. Carbon is one of the most common carriers widely used in fuel cells and batteries[74-76]. Yang *et al.* showed that Pt loading on sulfur-doped carbon support produced strong platinum-sulfur bonds, allowing small platinum alloy nanoparticles (< 5 nm in diameter) to be stabilized at temperatures up to 1000 °C[77]. They use sulfur-doped carbon as a support for synthesized intermetallic libraries of small nanoparticles consisting of 46 combinations of platinum with 16 other metal elements. Other carbon supports, such as porous carbon, porous oxide/carbon composite and graphene, are also commonly used to synthesize various intermetallic nanocrystals. Ji *et al.* modified the surface of ordered mesoporous carbon (OMC) with sulfur and used the surface-modified OMC-S as catalyst support to prepare OMC-PtBi nanocrystals embedded in the porous structure of OMC[78]. Because the OMC has a connected pore structure, a high pore density and a specific surface area, and the sulfur has a strong affinity for metals, the metal precursor in solution can be adsorbed and combined into the pores of OMC, and the particle growth can be limited in the reduction process, to obtain ultra-fine dispersed metal nanocrystals. The resulting nanocrystals have a size of about 2-3 nm and a uniform size distribution. In addition, they also synthesized other intermetallic PtM (M = Pb, Pd, Ru) catalysts using this method.

Alternatively, intermetallic can be prepared at the interface of metal and support by strong metal-support interactions[79]. Generally, noble metal nanocrystals are carried by oxide support and converted into intermetallic compounds by reduction at high temperatures. For example, Pd NPs supported on ZnO, Ga_2O_3, or In_2O_3 were converted into intermetallic ZnPd, Ga_2Pd_5, and InPd. Bernal *et al.* reduced Pt/CeO_2 in H_2 atmosphere at 200-950 ℃ and observed the structural transformation using HRTEM[80]. They found that Pt nanocrystals loaded on CeO_2 were converted to the intermetallic compound $CePt_5$ after annealing at high temperatures. The method of synthesizing intermetallic compounds by the strong interfacial interaction between metal and oxide carrier surface usually requires a long annealing time at high temperatures to transform into an ordered structure, so it is still challenging to apply this method to the synthesis of intermetallic compounds nanocrystals.

Coating-assisted annealing. By coating the nanocrystals with polymers, oxide protective layers (SiO_2, MgO) and KCl substrates, the diffusion between nanocrystals can be eliminated, thus effectively alleviating agglomeration and sintering during thermal annealing and precisely controlling the size of nanocrystals[81]. Fujimori *et al.* coated the surface of disordered face-centered cubic (*fcc*)-FePt with SiO_2 and subsequently thermally annealed to obtain ordered $L1_0$-FePt nanocrystals[82]. SiO_2 can limit the diffusion of Fe and Pt atoms during annealing, and the resulting material has an average particle size of 6.4 nm. Kim *et al.* used a similar approach coating the disordered *fcc*-FePt with a MgO protective layer (FePt/MgO), and heat-treated it at 800 °C to obtain an intermetallic FePt with an ordered face-centered tetragonal (*fct*) structure[83]. Song *et al.* developed a small molecule-assisted impregnation approach to realize the general synthesis of a family of Pt-based intermetallics[84]. They utilized molecular additives containing functional groups as ligands to coordinate Pt (IV) in impregnation, and then thermally converted to intermetallic nanoparticles coated on a hybrid atom-doped graphene layer. The method realized the general synthesis of 18 binary intermetallics, including Pt_3M (M = Ti, V, Cr, Mn, Fe, Co, Al, Ga, In, Ge, Sn), PtM (M = Mn, Fe, Co, Ni, Cu, Zn) and $PtCu_3$. Other inorganic salts such as NaCl and KCl were also able to stabilize nanoparticles during high-temperature annealing. However, these salts do not form a tight shell around each nanoparticle and are less efficient in stabilizing nanoparticles to prevent aggregation/sintering[85,86].

Defect-assisted annealing. The complete transition from disorder to order can also be achieved by introducing defects to lower the atomic diffusion barrier and promote mutual diffusion between metal atoms[87]. At present, defects are mainly introduced into the crystal interior by the generation of oxygen vacancies or by the introduction of a third element[88]. Sun *et al.* prepared disordered *fcc*-FePt-Fe_3O_4 nanocrystals by controlling the decomposition of $Fe(CO)_5$ and reduction of $Pt(acac)_2$, and obtained fully ordered *fct*-FePt nanocrystals by subsequent thermal annealing[89]. In the synthesis process, *fcc*-FePt NPs were first synthesized and then oxidized in air to obtain dumbbell *fcc*-FePt-Fe_3O_4 NPs, which were surrounded by a polycrystalline Fe_3O_4 shell. Then defects are generated when Fe_3O_4 is reduced to Fe, and the dumbbell structure ensures that Fe/Pt is easy to diffuse to form a fully ordered *fct* structure[90]. Wang *et al.* used a bifunctional core/shell Pt/$NiCoO_x$ as a precursor system to prepare sub-6 nm monodisperse ordered $L1_0$-$PtNi_{0.8}Co_{0.2}$ nanocrystals. $NiCoO_x$ can provide abundant oxygen vacancies to promote the diffusion of Pt/Ni/Co atoms and act as a protective shell to inhibit the sintering of nanocrystalline during thermal annealing[91].

Metallothermic reduction

Thermal reduction is a method of producing intermetallic compounds by reducing a metal source at high temperatures with a reducing agent [Figure 5B]. Usually, metal oxides, halides, or sulfides are used as metal sources, reducing gases (H_2, B_2H_6), and active metals (K, Mg, Al, Sn) as reducing agents. Due to the wide variety of reducing agents available in this method, many typical reactions have been developed, including solid-state metathesis reactions and metal thermal reduction reactions, to achieve the simple, rapid or universal synthesis of intermetallic compounds. Recently, our group has prepared a series of intermetallic borides and silicides by thermal reduction[92,93]. Our group employed the boron thermal reaction between boron powder and metal oxide under KCl-NaCl molten salt conditions to prepare phase-pure borides. Twelve single metals MB_2 (M= Ti, V, Cr, Mn, Zr, Nb, Mo, Hf, Ta, W, Re and Ru) were prepared by this method at relatively low temperatures (900-1000 ℃)[94]. The twelve metal diborides adopt four types of crystal structures. Their conspicuous structural difference lies in the different two-dimensional covalent boron sheet subunits. Later, we developed a solid-state metathesis reaction using magnesium diboride (MgB_2) and anhydrous metal chloride as feedstocks to produce intermetallic borides[95]. Due to the formation of a thermodynamically stable byproduct ($MgCl_2$), only a lower heating temperature is required. In addition, additional reducing agents can reduce residual boron impurities or other unwanted boride phases in the target product[23]. Our group reported the synthesis of mono-borides with Mg as an additional

reducing agent to reduce MCl_x under relatively mild conditions[96].

Wet chemistry method

Compared with the thermal annealing method, the wet chemical method is easier to control the morphology and size of metal compounds [Figure 5C]. In wet chemistry, intermetallic compounds are synthesized by direct reaction with the addition of precursors, reducing agents, capping agents, and surfactants in solution. Because high-temperature annealing is not required, particle agglomeration during annealing is avoided. However, due to the limitation of the boiling point of the solvent, the reaction can only be carried out at a low temperature, so it is necessary to adopt a suitable strategy to reduce the barrier of the transition from disordered alloys to ordered intermetallic compounds. The following two strategies can be adopted for the preparation of intermetallics[97].

(i) Adding halide ions (Cl^-, Br^-, I^-) or strong reducing agents (ascorbic acid (AA), tetrabutylammonium bromide (TBAB), $NaBH_4$) to the reaction solution to slow down the crystal growth rate. Rong *et al.* synthesized surface defect-rich Pt_3Sn using $Pt(acac)_2$ and $SnCl_2{\cdot}2H_2O$ as metal precursors, polyvinylpyrrolidone (PVP) as surfactant, and N, N-dimethylformamide (DMF) as solvent and reducing agent[98]. During synthesis, Cl^- released from $SnCl_2$ slows crystal growth and cooperates with O_2 to etch the nanocrystals. According to the growth-etching synergetic growth mechanism reported by Tilley, the corrosion process proceeds synchronously with the growth process in the presence of higher concentrations of corrosive agents. At the beginning of the reaction, the etching process is slow because the concentration of Cl^- in the solution is low. However, with Sn atoms reduced, more Cl^- is released into the solution, which leads to a faster etching rate and more defect formation. The newly generated Sn atoms can diffuse from the surface into the Pt-rich lattice to form PtSn solid solution. Liao *et al.* synthesized novel PtBi nanoplatelets (NPLs) and PdBi nanowires (NWs) with controlled shape, size, and composition in the presence of oleylamine (OAm) and NH_4Br[99]. Using a strong reducing agent, the simultaneous reduction of two metal precursors is also a method of synthesizing intermetallic compounds. Maksimuk *et al.* used TBAB as a reducing agent to simultaneously reduce $Pt(acac)_2$ and $Pb(acac)_2$ to synthesize ordered metal-interstitial PtPb nanorods[100]. Cable *et al.* reported the synthesis of a series of tin intergeneric compounds using $NaBH_4$ as a strong reducing agent[101].

(ii) By seed-mediated synthesis, metal nanocrystals with well-defined size, shape and composition are first synthesized, and then the second metal is diffused into the synthesized seeds by diffusion growth[102] [Figure 5D]. This synthesis strategy was pioneered by Cable and Schaak, who first reported the generation of intermetallic M-Zn nanocrystals (M = Au, Cu, and Pd) by seed-mediated diffusion growth using zero-valent Zn precursors in a hot organic amine solvent. Samanta *et al.* synthesized ultra-small monodisperse intermetallic NiZn nanoparticles by converting Ni nanoparticles into an ordered alloy using diethylzinc $[Zn(C_2H_5)_2]$ as precursor[103]. During the transformation, the particles retained their morphology, and the estimated particle size of the NiZn NPs was ~4.5 nm. The seed-mediated growth approach enabled the preparation of a variety of noble (gold, silver, platinum, and palladium) and non-noble (tin, plumbum, and copper) intermetallic compounds, and can realize the control of morphology. An excellent example was demonstrated in the solution-phase synthesis of core/shell PbPt/Pt with PbPt core being in hexagonal structure[104]. The core/shell NPs were made by using $Pt(acac)_2$ and $Pb(acac)_2$ as the metal precursors, oleylamine (OAm)/octadecene (ODE) mixture as solvents and surfactants, and AA as the reducing agent. Under the reaction condition, Pb was first reduced and Pt was deposited on the Pb seeds, followed by controlled Pt diffusion into the Pb seeds. With the Pb/Pt ratio controlled at about 1:1, hexagonal PbPt was obtained. Meanwhile, the authors found that using AA as a reducing agent was the key to forming a well-organized Pt atomic layer, because AA can be used as a weak acid to remove Pb during synthesis, allowing Pt atoms to diffuse and rearrange at higher temperatures.

Using Au nanocrystals as precursors, Chen *et al.* prepared monodisperse CuAu and Cu_3Au nanocrystals by seed diffusion method[105]. They prepared Cu_3Au and CuAu using 6.3 nm and 8.5-9.5 nm Au seeds at different temperatures, respectively. According to powder X-ray diffraction (XRD) patterns of the product, Cu_3Au intermetallic compounds of cubic order were formed at 300 °C when the Cu/Au atomic ratio was 3:1. The intermetallic compound CuAu was obtained at 280 °C when an equal molar amount of raw material was used. In addition, Clarysse *et al.* report the development of a colloidal synthesis method based on amalgamation of monometallic nanocrystal seeds with low melting point metals, and have used this method to obtain uniform intermetallic nanocrystals of Au-Ga, Ag-Ga, Cu-Ga, Ni-Ga, Pd-Ga, Pd-In and Pd-Zn compounds[106]. They showed that besides Ga, other low melting point metals (In and Zn) could be used to synthesize intermetallic compounds.

Although many methods have been used to synthesize intermetallics, they have sufficiently different advantages and disadvantages. For example, metallothermic reduction can synthesize highly-crystalline intermetallics that are difficult to obtain by wet chemical methods, such as silicates and borides, but the size of the as-synthesized products is still relatively large, dozens or hundreds of nanometers[93]. Wet chemical method can accurately control the morphology and size of intermetallics, but may involve some expensive metallic reagents [e.g., $Pt(acac)_2$, $Pd(acac)_2$] and auxiliary solvents (e.g., oleylamine, benzyl alcohol), resulting in high synthesis cost and difficulty in large-scale synthesis[97]. A significant trend for large-scale production of intermetallic catalysts is the development of green and low-cost synthesis of small-size intermetallic nanoparticles. In addition, the current synthesis of intermetallics mainly relies on trial-and-error approaches, which are inefficient and tedious. More research is needed on general methods and design principles for the synthesis of intermetallic phases.

ELECTROCATALYTIC APPLICATION OF INTERMETALLICS

The subsequent section mainly discusses important electrocatalytic reactions catalyzed by intermetallics, including HER, ORR, CO_2RR, and NRR. Readers who may seek detailed catalytic mechanisms of these electrocatalytic reactions are advised to consult several comprehensive reviews published elsewhere[107-109]. In this section, we do not intend to reiterate them, but rather concentrate on the developments of novel intermetallic electrocatalysts and structure-activity relationships.

Intermetallic electrocatalysts for HER

Water electrolysis is one of the promising technologies that can produce clean fuel hydrogen on a large scale. As a key half-reaction in water electrolysis, the HER at cathode usually requires an efficient electrocatalyst to reduce the reaction barrier and energy consumption. Noble metal Pt is readily recognized as the most active HER catalyst, but its high cost and scarcity hinder the wide commercialization of water electrolysis technology[110]. Alloying Pt with non-noble metals is an effective way to reduce Pt content and improve the intrinsic activity of electrocatalysts. In recent years, researchers have developed a series of Pt-based intermetallics, such as Pt_3Ti[111], PtFe[112], PtNi[113], Pt_3Co[114], and so on, whose ligand effects and stress effects between Pt and metal elements can regulate the surface adsorption properties, thus achieving the purpose of enhancing HER activity. For example, Zhang *et al.* reported an IrMo intermetallics supported on carbon nanotubes by a hydrogel-freeze-drying method, whose specific activity for HER was 9.5 folds that of Pt/C[115]. The stably-adsorbed OH spectator on the Mo site optimized the surface chemical environment and electronic structure of the catalyst, resulting in superior hydrogen adsorption energy and accelerating the water dissociation kinetics.

Developing non-Pt HER catalysts with Pt-like activity has been an important research direction in recent years. Especially, some noble metal-based intermetallics, such as Ru (RuB_2, RuB, RuSi, RuGe, *etc.*),[93,116,117] Pd

(Pd_2B, PdSi, *etc.*)[118,119], Rh (RhB, RhSi, *etc.*)[120] and Ir (IrMo, IrSi, *etc.*)[121-123] have attracted wide attention. Our group studied a series of light element (e.g., Si, B)-containing intermetallics (silicide and boride), and found that the hybridization between *sp* orbital of light elements and *d* orbital of transition metals dominates the electronic structure characteristics [Figure 6A][96,118,124]. This *sp-d* orbital hybridization can reduce the hydrogen adsorption energy of metal surface and regulate the catalytic activity for HER [Figure 6B]. Based on these understandings, several non-Pt HER electrocatalysts with Pt-like activity, such as RuB and RuSi, have been confirmed by experiments and theoretical calculations [Figure 6B][96,118,124]. Inspired by these works, the discovery of new synthesis methods and novel electrocatalysts based on borides and silicide intermetallics has become a hot topic in recent years[120,121,125,126].

Compared with the disordered alloys, the intermetallic structures would not only enhance the catalytic activity, but also possess greater structural stability during HER. A remarkable example is Pd-B alloys reported by our group [Figure 6C][118]. Controlled preparation of intermetallic Pd_2B and disordered Pd-B alloys was achieved by temperature control in a metallothermic reduction reaction. Despite a similar stoichiometric ratio, the intermetallic Pd_2B exhibits significantly higher catalytic activity for HER than the disordered Pd-B alloy, because the interstitial boron ordering of the former yields an optimal near-surface electronic structure. Moreover, the catalytic and structural stability of intermetallic Pd_2B is significantly enhanced relative to the disordered Pd-B alloy. (i) The leaching amount of B from Pd_2B (1.4%) is less than that of disordered Pd-B alloy (13.3%) during HER. (ii) Pd_2B possesses excellent catalytic stability for more than 7 days, while the disordered Pd-B alloy suffers severe deactivation.

In order to further reduce the amounts of noble metals and optimize catalytic performance in noble metal-based intermetallics, several important strategies have been developed. One strategy is to load noble metal intermetallics onto a suitable support, for example, IrGa supported on nitrogen-doped reduced graphene oxide,[127] Pt_3Ti nanoparticles supported on $Ti_3C_2T_x$[111]. In these supported catalysts, in addition to reducing the amount of noble metals, the support effects can improve HER catalytic performance through metal-support electronic interaction. Another effective strategy to promote the catalytic performance of intermetallics is accurate nanostructure design. For example, Liu *et al.* prepared a series of ordered mesoporous PtZnM trimetals (M= Sc, V, Cr, Mn, Fe, Co, Ni, Cu or Ga) through a concurrent template route [Figure 6D and E][128]. Among them, the PtZnCo trimetals display a higher mass activity (0.36 A mg_{pt}^{-1} at -0.05 V) for HER than that of commercial Pt/C (0.22 A mg_{pt}^{-1}) and strong catalytic stability for 50000 cycles, attributing to the large specific surface area and abundant low coordination active sites.

The ultimate pursuit of HER electrocatalysts is to develop highly active, noble metal-free catalysts. Intermetallic electrocatalysts based on Mo, W, Fe, Co, Ni and other non-noble metals have been widely studied, such as Gd_2Co_{17}[129], Co_7Mo_6[130], NiZn[131], and Co_3W[132]. Although an enormous number of non-noble metal intermetallic electrocatalysts have been reported, it should be pointed out that their intrinsic activities for HER are usually 1-2 orders of magnitude lower than those of Pt-based catalysts[133]. Their high catalytic activities are often achieved at high loadings or/and large surface areas of catalysts to compensate for relatively worse intrinsic activity. Moreover, these non-noble metal electrocatalysts face a larger challenge in long-term catalytic stability relative to Pt/C catalysts.

Intermetallic electrocatalysts for ORR

ORR is an important half-reaction in fuel cell technology. The reaction largely determines the overall efficiency of fuel cells, because of multiple proton-electron transfer and sluggish reaction kinetics[134]. Similar to HER electrocatalysis, noble metal Pt is traditionally the most active electrocatalyst for ORR[43]. Alloying is an effective strategy to reduce the amount of Pt and increase the catalytic activity of ORR[135]. The strain and

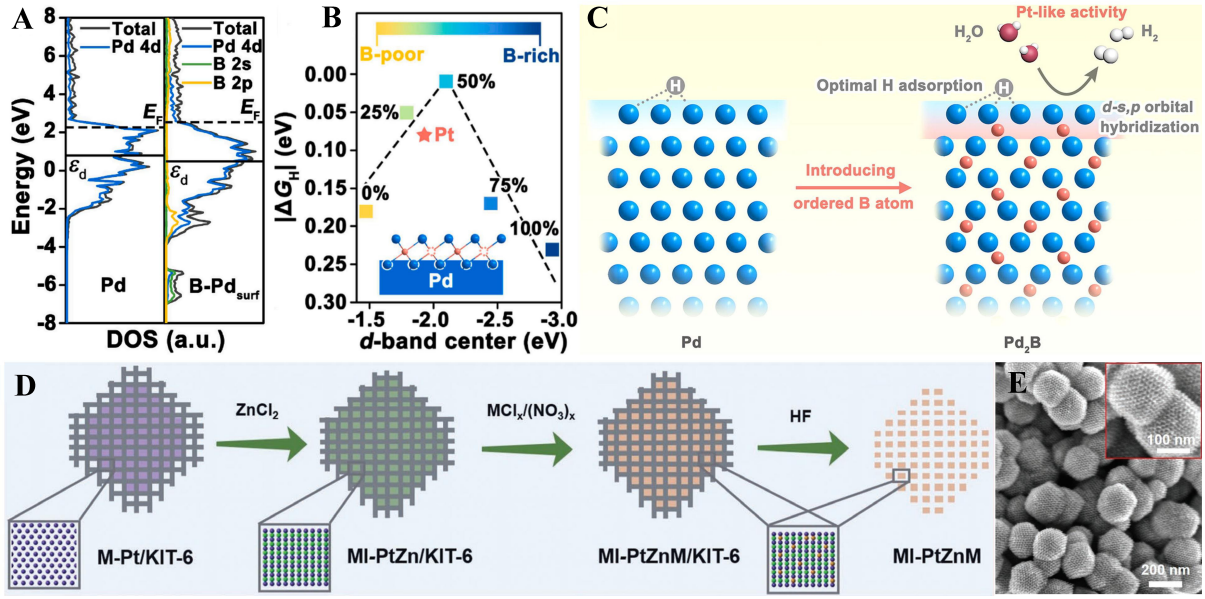

Figure 6. (A) Calculated *p*DOS of Pd and Pd-B alloy models; (B) A volcano plot showing the ΔG_H. values of Pd-B alloy models containing different subsurface B concentrations as a function of their surface *d*-band centers. The inset shows the structural model of Pd-B systems with different subsurface B concentrations; (C) Schematic illustration of ordered interstitial B atom in Pd_2B electrocatalysts and the optimal near-surface electronic structure for HER[118]; (D) Schematic illustration of the synthesis of ordered mesoporous PtZnM trimetals[128]; (E) Scanning electron microscopy (SEM) image of ordered mesoporous PtZnCo trimetals.

ligand effects in Pt alloys can influence the electronic structure and surface adsorption behavior, leading to greater catalytic activity for ORR. However, Pt alloys often suffer from poor stability, which is assigned to corrosion and leaching of transition metals during the catalytic process. The dissolved metal cations hinder proton conduction and accelerate the decomposition of the membrane and catalytic surface. Unlike the disordered Pt-M alloys, Pt-based intermetallics exhibit enhanced chemical stability in operating conditions due to ordered atomic arrangement and strong bonding interactions. The Pt-based intermetallics are expected to be new-generation ORR catalysts to realize low cost, greater catalytic activity and long-term durability simultaneously.

The exploration of Pt-based intermetallics as ORR electrocatalysts has progressively covered Pt-transition metal alloys (e.g., Pt_3Ni, Pt_3Co, Pt_3Mn, Pt_3Cu),[136-138] Pt-rare earth alloys (e.g., Pt_3Y, Pt_5La)[139-141], Pt-alkaline earth alloys (e.g., Pt_5Ca and Pt_5Sr)[142] and so on. A typical class of Pt-based intermetallic catalysts for ORR is binary Pt_3M (M = 3d-transition metals). In 2007, Stamenkovic *et al.* demonstrated a volcano-type relationship between the surface electronic structure and ORR activity for Pt-transition metal alloys Pt_3M (M=Ni, Co, Fe, Ti, V)[143]. The Pt_3Ni and Pt_3Fe are found to be at the very top of the volcano plot, exhibiting better ORR activities compared with pure Pt. In 2014, Yang *et al.* synthesized hollow Pt_3Ni nanoframes with open structures and high surface areas, which displayed 36 times higher mass activity than Pt/C catalysts[144]. Subsequently, some doping and heterostructure strategies are developed to realize the component and structure optimization of Pt_3Ni catalysts for ORR, such as Mo-doped Pt_3Ni octahedron, Ni_3C@Pt_3Ni core-shell nanoparticles[145].

Constructing of ultrathin Pt shell on the surface of Pt-based intermetallic nanoalloys is an important strategy to improve the ORR activity. The formation of core-shell structure (such as PtPb/Pt, PtCo@Pt, *etc.*) can regulate the d-band center of the surface Pt atoms, thus changing the binding strength between the electrocatalyst surface and oxygen intermediates[138,146,147]. Recently, the Yang group proposed a Co_3O_4-

assisted structural evolution strategy [Figure 7A] to controllably synthesize sub-6 nm core-shell Pt_1Co_1 intermetallic compound(Pt_1Co_1@Pt)[148]. Experiments and theoretical calculations showed that the ordered arrangement of Pt-Co atoms reduced the d-band center of surface Pt relative to the pure Pt and enhanced the oxidation resistance of Pt/Co sites, thus improving the ORR activity and durability. The proton exchange membrane fuel cell (PEMFC) using Pt_1Co_1@Pt as cathode catalyst layers exhibited a record power density (2.30/1.23 W cm^{-2} under H_2-O_2/air conditions) and extraordinary stability, making it the highest performance fuel cell of the time.

The synthesis of Pt-based intermetallics often requires high-temperature annealing to overcome the kinetic energy barrier of atomic ordering rearrangement in the solid phase. However, high-temperature synthesis inevitably leads to serious sintering of metal particles and a decrease in surface area, which ultimately results in low overall activity. It is highly desirable yet challenging to develop synthetic methods for small-sized Pt-based intermetallic catalysts. The Liang group developed a high-temperature sulfur anchoring synthesis strategy to construct an intermetallic library composed of 46 small-sized Pt-based intermetallic nanoparticles (< 5 nm), including 20 binary and 26 multicomponent intermetallics on sulfur-doped carbon supports [Figure 7B and C][77]. The strong interaction between Pt atoms and S atoms on carbon supports inhibits metal sintering during high-temperature annealing. Among them, the PtCo and PtNi catalysts showed mass activities of 1.52 and 1.84 A mg_{Pt}^{-1}, which was much higher than commercial Pt/C catalyst (0.29 A mg_{Pt}^{-1}) in H_2-O_2 cell tests at 0.9 volts. Subsequently, the Liang group realized the grams scale production of Pt-intermetallic catalysts on commercial carbon black supports by a small molecule-assisted impregnation method[84,149]. This work is an important step towards the practical application of nano-sized Pt-intermetallic catalysts.

Pd is considered the most suitable alternative to Pt catalyst for ORR, because Pd has similar physical and electrochemical properties to Pt and is relatively inexpensive. The ORR properties of Pd-based intermetallics have been widely studied, such as PdCu,[150] Pd_3Pb[151], and Pd_6Ni[152]. Huang *et al.* reported a template-directed rapid synthesis method [Figure 7D and E] for a series of Pd-based ultra-thin porous intermetallic Pd-M nanosheets (M = Pb, Sn and Cd)[153]. The mass activity and specific activity of Pd_3Pb catalysts are 6.8 times and 9.8 times that of commercial Pt/C in the alkaline medium for ORR, respectively. Recently, Hu *et al.* reported a novel technique for the synthesis of intermetallic Pd_3Pb nanoparticles by rapid joule heating within 60 s[154]. The short heating time can prevent particle aggregation, thus realizing the loading of ultra-small Pd_3Pb nanoparticles with a narrow size distribution (6 nm) on carbon fiber supports. The synthesized Pd_3Pb nanoparticles showed greater electrocatalytic activity for ORR than traditionally heated Pd_3Pb.

Intermetallic electrocatalysts for CO_2RR

Electrochemical CO_2RR provides an attractive approach for the reduction of greenhouse gas emissions and the production of high-value-added industrial products[155-157]. The CO_2RR in H_2O electrolyte can be described as multiple steps of proton-coupled electron transfer and yields a range of different products, such as formates, CO, and hydrocarbons[158]. Many metal catalysts for CO_2RR have been explored, which can be classified into three categories according to their main products: CO (Ag, Au, Zn, *etc.*), formates (Bi, Sn, Hg, In, *etc.*) ,and hydrocarbons (Cu)[159]. However, most monometallic catalysts are undesirable for CO_2RR in terms of efficiency and selectivity. Intermetallic alloys provide unique electronic structures and well-defined coordination environments for precise tuning of catalytic activity and selectivity of CO_2RR[21,28,29,153,160]. A broad range of nanostructured intermetallic catalysts has been developed for electrochemical CO_2RR[161].

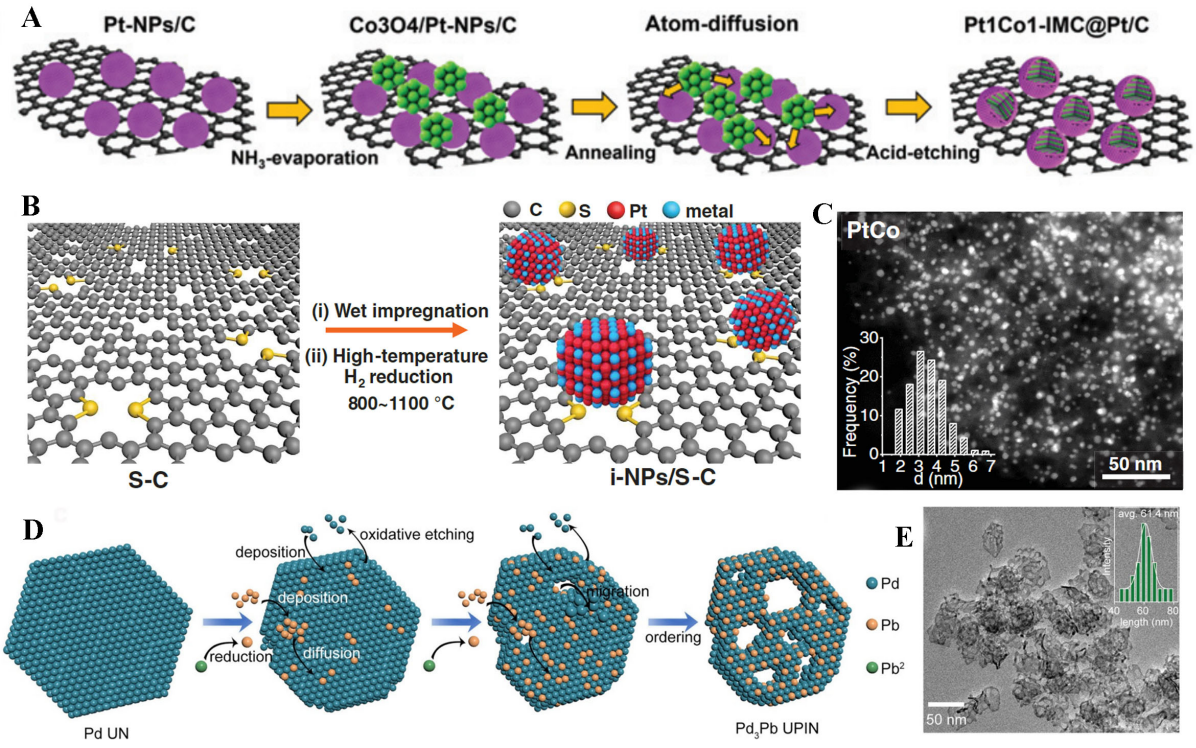

Figure 7. (A) Schematic illustration of the synthesis of Pt_1Co_1@Pt[148]; (B) Schematic illustration of the general synthesis of 46 Pt-based intermetallic nanoparticles on porous sulfur-doped carbon supports[77]; (C) The transmission electron microscopy (TEM) image of intermetallic PtCo nanoparticles; (D) Schematic illustration of the template-directed synthesis of porous intermetallic Pd-M nanosheets[153]; (E) The TEM image of intermetallic Pd_3Pb nanosheets.

Compared to monometallic catalysts, intermetallic alloys can improve the catalytic activity. For example, Sn catalysts can only exhibit low CO_2RR selectivity within a narrow potential window for formate generation, due to the large energy barriers and slow kinetics of the oxygen-breaking hydrogenation and desorption steps[162,163]. Tan *et al.* reported an ordered nanoporous intermetallic SnTe, which has better electrochemical CO_2 to formate reduction performance compared to monometallic Sn catalysts[164]. This SnTe maintains more than 90% Faraday efficiency (FE) over a voltage range of -1.0 to -1.3 V (vs RHE). Combining operando Raman spectroscopy analysis with DFT calculation, it is found that the strong orbital interaction between Sn and neighboring Te in the intermetallic SnTe promotes bond breaking between metal and oxygen, which significantly increases the yield of formate. In addition, Jiang *et al.* synthesized a self-supported nanoporous Cu-Sn hybrid electrode, which is an intermetallic Cu_3Sn *in situ* formed on Cu skeleton (Cu_3Sn/Cu)[165]. Due to the enhanced adsorption ability of CO on Cu atoms, the intrinsic activity of Cu_3Sn is 80 times higher than that of monometallic Cu, with a FE of 91.5% and excellent selectivity at an overpotential of 0.59 V.

Besides catalytic activity, the product selectivity of CO_2RR can be changed by the rational construction of intermetallic catalysts. For example, Yang *et al.* investigated the effect of disorder-to-order transformation for AuCu bimetallic nanoparticles on their CO_2RR selectivity [Figure 8A][166]. While the intermetallic AuCu electrocatalysts selectively converted CO_2 to CO with a high Faraday efficiency of 80%, the disordered counterpart was mainly catalytically active for HER [Figure 8B and C]. DFT calculation and X-ray absorption analysis further confirmed that the increased activity and CO selectivity of ordered AuCu nanoparticles are due to the formation of a compressive strain Au shell layer over the AuCu intermetallic

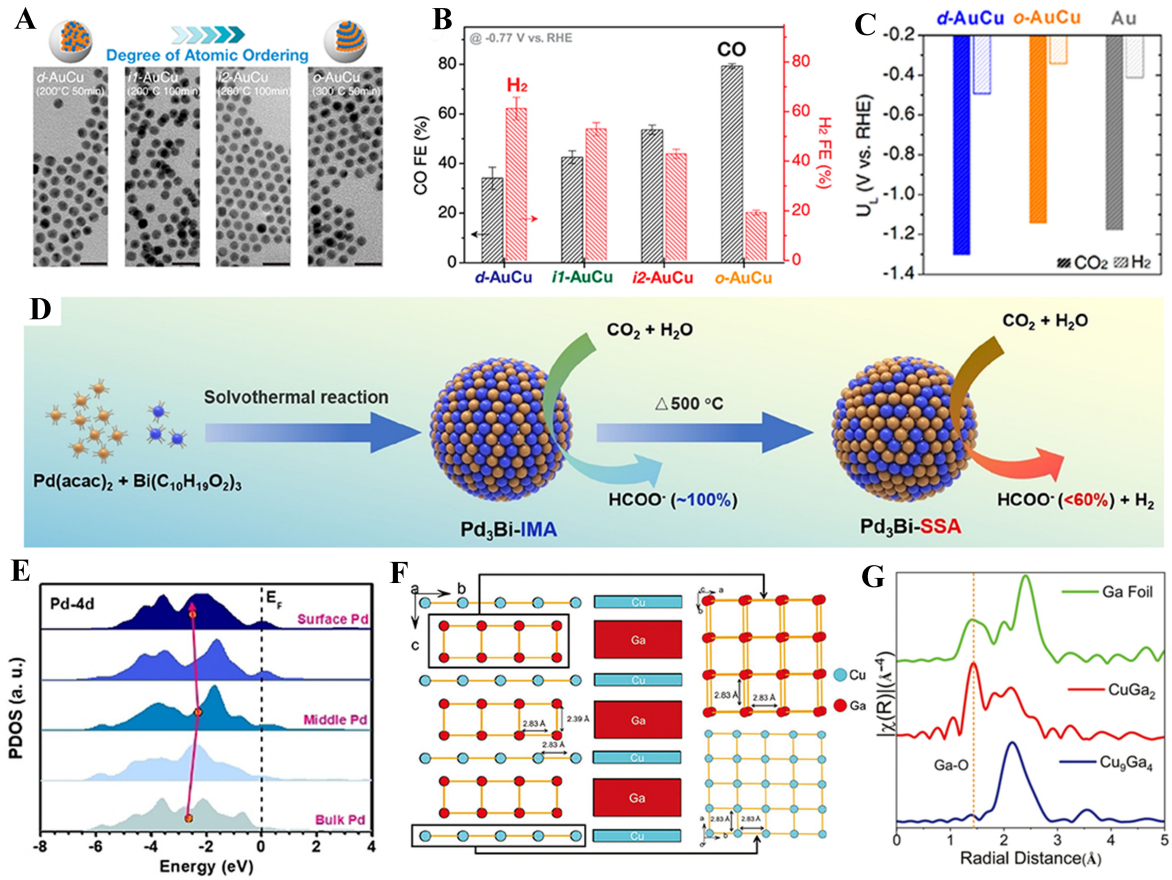

Figure 8. (A) TEM images of AuCu bimetallic nanoparticles with different ordering degrees[166]; (B) Electrochemical CO_2 reduction activities of AuCu nanoparticles evaluated by Faraday efficiencies of CO and H_2; (C) Calculated limiting potentials for CO_2 reduction and H_2 evolution; (D) Schematic synthetic procedures for intermetallic Pd_3Bi and disordered Pd_3Bi alloys[167]; (E) Site-dependent projected partial density of states of Pd-4d in intermetallic Pd_3Bi. (F) Crystal structure of $CuGa_2$[168]; (G) Comparison of normalized XANES spectra of Ga K-edge of $CuGa_2$ and Cu_9Ga_4 with the standard sample.

core. Another example is intermetallic Pd_3Bi nanocrystals and chemically disordered Pd_3Bi nanoparticles [Figure 8D and E] that were selectively synthesized by Li *et al.*[167]. The intermetallic Pd_3Bi exhibited excellent selectivity for formate generation (≈ 100%), while the formate selectivity of disordered Pd_3Bi reached only 60%. DFT calculation indicated that the crystallographic ordering of Pd and Bi atoms in Pd_3Bi can inhibit the *CO poisoning and improve *OCHO adsorption during CO_2RR to formate.

For intermetallic catalysts, phase structures have a significant effect on the electrocatalytic performance of CO_2RR. Recently, Peter *et al.* prepared two intermetallic phases ($CuGa_2$ and Cu_9Ga_4) formed by copper and gallium through a high-temperature solid-state reaction for electrocatalytic CO_2RR [Figure 8F and G][168]. While the $CuGa_2$ achieved a selective reduction of CO_2 to methanol at a very low potential of -0.3 V with a Faraday efficiency of 77.26%, the Cu_9Ga_4 showed a much lower Faraday efficiency (37.75%) to produce methanol. The higher catalytic performance of $CuGa_2$ is found to attribute to its unique two-dimensional structure, which preserves surface and subsurface oxide species (Ga_2O_3) in the reducing atmosphere.

Intermetallic electrocatalysts for NRR

Industrial ammonia synthesis relies substantially on the Haber-Bosch reaction, which involves a massive energy input and emits large amounts of greenhouse gases[169]. The electrochemical NRR under ambient conditions provides an attractive route to realize green ammonia synthesis. Efficient NRR electrocatalysts are highly required to break the inert nonpolar N≡N triple bond of a N_2 molecule and to inhibit severe competition from the HER in H_2O electrolyte[170-172]. Intermetallic nanocrystals have been widely investigated in the NRR field to exhibit excellent catalytic properties and good stability. The synergistic atomic interaction in intermetallic compounds can modulate the adsorption and desorption of N-containing intermediates while suppressing the competing process of HER, resulting in a lower reaction energy barrier and superior catalytic activity[51].

Many theoretical computational studies have been reported to accelerate the discovery of intermetallic catalysts with desirable NRR properties[19,173]. Yuan *et al.* calculated the N adsorption behavior on the surface of 29 intermetallics with Cu_3Au-type structures[174]. Among the calculated intermetallics, Pd_3Mo was considered as an attractive catalyst with a low limiting potential of -0.31 V and the ability to suppress the competing HER. Some theoretical studies have suggested that some unique structures of intermetallic compounds can provide ideal single-atom nonmetallic sites for efficient NRR. For example, the Qiao group simulated molybdenum boride models (e.g., Mo_2B, α-MoB and MoB_2) to explore their NRR activities[175]. Electronic structure studies showed that the occupancy of the hybridized orbital between the *p*-orbital of the boron site and the antibonding π^*-orbital of N_2 determined the binding strength of N_2, so that the filling of the p_z-orbital could be accepted as a descriptor of N_2 activation [Figure 9A and B]. With increased boron content, the filling of p_z-orbital increased in different Mo-B phases. The p_z-orbital of Mo_2B phase containing isolated boron sites is less filled, thus promoting the activation of N_2. Moreover, this conception of isolated boron site is equally applicable in other metal borides in the form of M_2B (M=Ti, Cr, Mn, Fe, Co, Ni, Ta, W). Due to the moderately filled p_z-orbital and the high adsorption strength of the reaction intermediates, Mo_2B, Fe_2B and Co_2B can be potential catalyst candidates for NRR.

Very recently, our group simulated anti-perovskite boride models with metal-coordinating single boron sites ($M_3M'B$) to reveal the effect of a boron-centered local environment [Figure 9C] on the catalysis of N_2-NH_3[176]. DFT calculation demonstrates that whereas the adsorption and activation of dinitrogen depend on the presence of isolated boron atoms on the surface, the adsorption conformation of dinitrogen is strongly dependent on the type of M atoms. The M atoms and isolated boron atoms work collectively to stabilize the N_xH_y intermediates for diazo conversion, and M' atoms can modulate the orbital hybridization of the B-M complex, thereby controlling the surface chemisorption and catalytic activity of the *N intermediates. Finally, we predicted that Rh_3GeB, Rh_3SbB and Ni_3LiB are the promising catalysts for ammonia synthesis with higher activity than the Ru (0001) surface.

Apart from theoretical studies, it was confirmed by experimental studies that some intermetallic compounds can work as highly active NRR catalysts[177-179]. Tan *et al.* prepared nanoporous intermetallic Pd_3Bi with strong Pd-Bi coupling by transforming chemically etched $PdBi_2$ [Figure 9D and E][180]. The Bi sites in Pd_3Bi can adsorb N_2 molecules and lower the energy barrier of $*N_2$ [Figure 9F]. Simultaneously, the bicontinuous nanoporous structure of the Pd_3Bi can accelerate the electron transfer in NRR and further improve NRR performance. As a result, the Pd_3Bi can exhibit a high NH_3 yield rate of 59 μg h^{-1} mg_{cat}^{-1} and a high Faraday efficiency of 21.5% at -0.2 V. Additionally, Sun *et al.* reported the preparation of Mo_3Si thin films on graphite paper by the magnetron sputtering technique[181]. Electrochemical tests demonstrated that Mo_3Si is an efficient NRR catalyst with high structural stability and exceptional selectivity for NH_3 production. DFT calculation indicated that the exposed Mo ions show high chemical activity to facilitate the activation and adsorption of N_2.

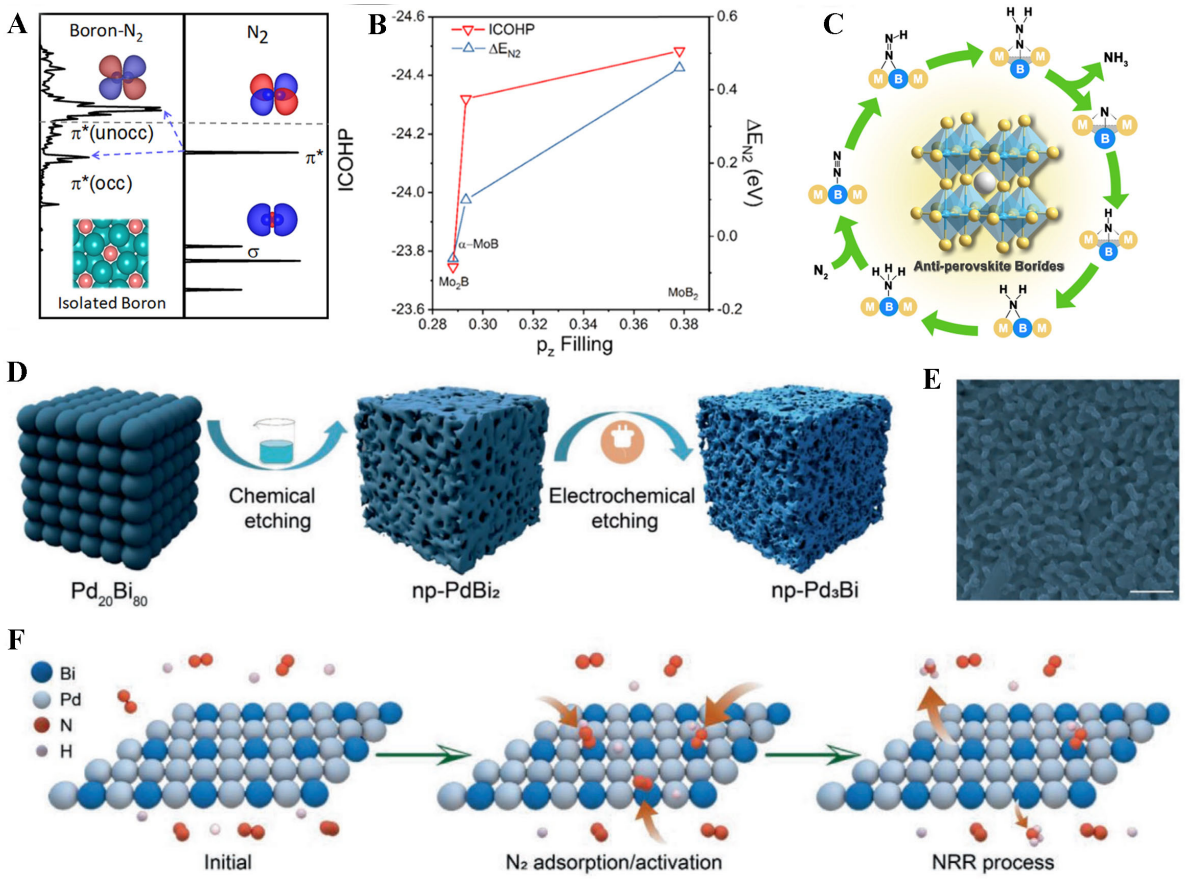

Figure 9. (A) Schematic illustrations of hybridization interactions between the boron p-orbital of Mo_2B and the π^*-orbital of the N_2 molecule; (B) Correlation between p_z-orbital filling with ICOHP and adsorption energy of N_2 [175]; (C) Schematic illustrations of single-boron sites confined in antiperovskite borides for NRR[176]; (D) Schematic illustration of the synthesis of nanoporous intermetallic Pd_3Bi[180]; (E) The SEM image of nanoporous Pd_3Bi; (F) schematic illustration of the NRR process on Pd_3Bi.

Although great achievements have been made, several unresolved questions still should be addressed in the catalytic application of intermetallics. (i) Current electrocatalytic studies of intermetallics mainly focus on HER and ORR. There is still insufficient research on CO_2RR and NRR electrocatalysis of intermetallic catalysts. (ii) Mechanistic investigations are scant and unsystematic for intermetallic catalysts, which generally possess complex surface structures and diverse active site motifs. Combining advanced characterizations with density functional theory (DFT) calculation, an in-depth understanding of structure-performance relationships at the atomic and electronic levels is highly required. (iii) Although a variety of intermetallic catalysts have been developed, their high activities are measured by three-electrode system, and have rarely translated into electrochemical devices such as fuel cells and water electrolyzers. Thus, establishing reasonable performance evaluation criteria is essential to bridge the gap between three-electrode and device tests.

CONCLUSION AND OUTLOOK

Intermetallic compounds exhibit superior activity and stability compared to traditional disordered alloy catalysts, owing to their ordered atomic arrangement which allows for precise regulation of electronic structure and generation of new active sites. As a result, intermetallic compounds offer a promising platform for studying the structure-property relationships, including the geometric effects and electronic effects. This paper provides a clear definition of intermetallic compounds, and comprehensively summarizes

the fundamental principles, common synthesis methods, and various electrocatalytic applications of intermetallic compounds. Despite the significant progress achieved in the synthesis and catalysis of ordered intermetallic compounds as reported in this paper, certain challenges must be overcome to realize the full potential of this novel material and meet the requirements of sustainable development.

The relationship between the structure and properties of intermetallic compounds is of critical importance for understanding their superior stability and activity in catalysis. However, during electrocatalysis, several significant structural changes, such as oxidation, surface reconstruction, disordered transformation, *etc.*, may occur, leading to alterations in the catalytic active site and affecting the properties of intermetallic compounds[182]. To obtain a complete understanding of these structural changes, advanced *in situ* methods such as *in situ* X-ray photoelectron spectroscopy (XPS), SEM, TEM, and extended X-ray absorption fine structure (EXAFS) are necessary to obtain spatial and temporal information on the atomic positions on the catalyst surface and bulk. The obtained information can support theoretical calculations and provide insights into the complete catalytic process. A comprehensive understanding of these steps is essential to elucidate the structure-property relationship, comprehend the impact of the ordered structure of intermetallic compounds on catalytic performance, and advance the catalytic applications of intermetallic compounds.

Developing more accurate, controllable, and rapid synthesis strategies for intermetallic compounds is crucial to fully leverage their potential in catalysis. Intermetallic compounds are known for their high thermodynamic stability due to their ordered structure, but the process of transitioning from a disordered to an ordered structure involves overcoming a high kinetic energy barrier, and therefore, synthesis conditions such as temperature, carrier, and precursor must be carefully regulated to minimize agglomeration caused by high temperatures. Alternatively, the synthesis temperature can be reduced by lowering the kinetic energy barrier. For example, introducing appropriate vacancies may also facilitate the rearrangement of atoms during the synthesis process. Meanwhile, intermetallic compounds may contain a series of crystalline phases with close stoichiometric ratios, such as Pd_2B, Pd_5B_2, and Pd_3B[183,184]. Even for a particular crystalline phase, intermetallic compounds usually give rise to multiple exposure surfaces. It is still a challenge to accurately obtain the crystalline phase of the pure phase and a specific exposure surface. This hinders the construction of model catalysts for in-depth analysis of structure-activity relationships, and it is urgent to develop more selective synthesis methods. Additionally, although Gibbs free energy and Arrhenius equation can provide guidance for the formation of intermetallic compounds, the mechanism and kinetics of the formation of ordered structures are not yet clear. Therefore, improving the fundamental understanding of the synthesis mechanism is necessary to precisely adjust the synthesis parameters and achieve optimal synthesis conditions.

Exploring more potential intermetallic compounds is essential to leverage their advantages in catalysis fully. Many binary intermetallic compounds have attracted extensive research interest; however, the current understanding of intermetallic compounds is limited, and the candidate space for these materials remains significantly unexplored. For example, developing new non-precious metals or polymetallic intermetallic compounds is of great significance to reduce the use of precious metals and enable large-scale energy conversion in the future. Moreover, combining emerging high-throughput and machine learning methods can accelerate the discovery of potential candidate intermetallic compounds and facilitate the screening of properties of existing intermetallic compounds. High-throughput methods involve the rapid screening of a large number of materials, allowing for the exploration of a wider range of materials. Machine learning algorithms can then be used to analyze the large amount of data generated by these methods to identify promising candidates and predict their properties. By leveraging these tools, researchers can accelerate the

discovery of new intermetallic compounds with desirable properties for catalysis and other applications. This approach has the potential to significantly increase our understanding of intermetallic compounds and enable the development of more efficient and cost-effective catalysts for a range of industrial processes.

DECLARATIONS

Authors' contributions

Prepared the manuscript: Zhang M, Liu Q, Sun W, Sun K, Shen Y, An W, Zhang L
Performed manuscript correcting: Chen H, Zou X

Availability of data and materials

Not applicable.

Financial support and sponsorship

This work was supported by the National Key R&D Program of China (2021YFB4000200) and the National Natural Science Foundation of China (NSFC) (21922507, 22179046).

Conflicts of interest

All authors declared that there are no conflicts of interest.

Ethical approval and consent to participate

Not applicable.

Consent for publication

Not applicable.

REFERENCES

1. Chen T, Foo C, Edman Tsang SC. Interstitial and substitutional light elements in transition metals for heterogeneous catalysis. *Chem Sci* 2020;12:517-32. DOI PubMed PMC
2. Chen H, Zhang B, Liang X, Zou X. Light alloying element-regulated noble metal catalysts for energy-related applications. *Chinese J Catal* 2022;43:611-35. DOI
3. Chen H, Zhang M, Wang Y, et al. Crystal phase engineering of electrocatalysts for energy conversions. *Nano Res* 2022;15:10194-217. DOI
4. Liang J, Ma F, Hwang S, et al. Atomic arrangement engineering of metallic nanocrystals for energy-conversion electrocatalysis. *Joule* 2019;3:956-91. DOI
5. Chen H, Wu Q, Wang Y, et al. Correction: d-sp orbital hybridization: a strategy for activity improvement of transition metal catalysts. *Chem Commun* 2022;58:7730-40. DOI PubMed
6. Nakaya Y, Furukawa S. Catalysis of alloys: classification, principles, and design for a variety of materials and reactions. *Chem Rev* 2023;123:5859-947. DOI PubMed
7. Zhou M, Li C, Fang J. Noble-Metal based random alloy and intermetallic nanocrystals: syntheses and applications. *Chem Rev* 2021;121:736-95. DOI
8. Furukawa S, Komatsu T, Shimizu K. Catalyst design concept based on a variety of alloy materials: a personal account and relevant studies. *J Mater Chem A* 2020;8:15620-45. DOI
9. Brown OW, Borland JB, Johnston RA, Grills RC. Catalytic activity of intermetallic compounds in the gas phase reduction of nitrobenzene. *J Phys Chem* 1939;43:805-7. DOI
10. Berk B, Brown OW. Catalytic activity of intermetallic compounds in the vapor-phase reduction of nitrobenzene. II. *J Phys Chem* 1942;46:964-8. DOI
11. Butler JN, Giner J, Parry JM. Some topics in electrocatalysis. *Surf Sci* 1969;18:140-58. DOI
12. Huq AKMS, Rosenberg AJ, Makrides AC. Electrochemical behavior of nickel compounds: II. Anodic dissolution and oxygen reduction in perchlorate solutions. *J Electrochem Soc* 1964;111:278. DOI
13. Justi EW, Ewe HH, Kalberlah AW, Saridakis NM, Schaefer MH. Electrocatalysis in the nickel titanium system. *Energy Conversion*

1970;10:183-7. DOI
14. Walter C, Menezes PW, Driess M. Perspective on intermetallics towards efficient electrocatalytic water-splitting. *Chem Sci* 2021;12:8603-31. DOI PubMed PMC
15. Miles MH. Evaluation of electrocatalysts for water electrolysis in alkaline solutions. *J Electroanal Chem Interf Electrochem* 1975;60:89-96. DOI
16. Jakšić M. Electrocatalysis of hydrogen evolution in the light of the brewer - engel theory for bonding in metals and intermetallic phases. *Electrochimica Acta* 1984;29:1539-50. DOI
17. Lu PWT, Srinivasan S. Nickel-based alloys as electrocatalysts for oxygen evolution from alkaline solutions. *J Electrochem Soc* 1978;125:265-70. DOI
18. Katoh A, Uchida H, Shibata M, Watanabe M. Design of electrocatalyst for CO_2 reduction: V . effect of the microcrystalline structures of Cu-Sn and Cu-Zn alloys on the electrocatalysis of CO_2 reduction. *J Electrochem Soc* 1994;141:2054-8. DOI
19. Abghoui Y, Garden AL, Howalt JG, Vegge T, Skúlason E. Electroreduction of N_2 to ammonia at ambient conditions on mononitrides of Zr, Nb, Cr, and V: A DFT Guide for experiments. *ACS Catal* 2016;6:635-46. DOI
20. Armbrüster M. Intermetallic compounds in catalysis - a versatile class of materials meets interesting challenges. *Sci Technol Adv Mater* 2020;21:303-22. DOI PubMed PMC
21. Rößner L, Armbrüster M. Electrochemical energy conversion on intermetallic compounds: a review. *ACS Catal* 2019;9:2018-62. DOI
22. Chen X, Liang C. Transition metal silicides: fundamentals, preparation and catalytic applications. *Catal Sci Technol* 2019;9:4785-820. DOI
23. Jothi PR, Yubuta K, Fokwa BPT. A simple, general synthetic route toward nanoscale transition metal borides. *Adv Mater* 2018;30:e1704181. DOI PubMed
24. Wang D, Peng Q, Li Y. Nanocrystalline intermetallics and alloys. *Nano Res* 2010;3:574-80. DOI
25. Kumar A, Dutta S, Kim S, et al. Solid-State reaction synthesis of nanoscale materials: strategies and applications. *Chem Rev* 2022;122:12748-863. DOI
26. Li J, Sun S. Intermetallic nanoparticles: synthetic control and their enhanced electrocatalysis. *Acc Chem Res* 2019;52:2015-25. DOI PubMed
27. Xiao W, Lei W, Gong M, Xin HL, Wang D. Recent advances of structurally ordered intermetallic nanoparticles for electrocatalysis. *ACS Catal* 2018;8:3237-56. DOI
28. Yan Y, Du JS, Gilroy KD, Yang D, Xia Y, Zhang H. Intermetallic nanocrystals: syntheses and catalytic applications. *Adv Mater* 2017;29:1605997. DOI PubMed
29. Furukawa S, Komatsu T. Intermetallic compounds: promising inorganic materials for well-structured and electronically modified reaction environments for efficient catalysis. *ACS Catal* 2017;7:735-65. DOI
30. Menezes PW, Walter C, Hausmann JN, et al. Boosting water oxidation through in situ electroconversion of manganese gallide: an intermetallic precursor approach. *Angew Chem Int Ed Engl* 2019;58:16569-74. DOI PubMed PMC
31. Hausmann JN, Beltrán-Suito R, Mebs S, et al. Evolving highly active oxidic iron(III) phase from corrosion of intermetallic iron silicide to master efficient electrocatalytic water oxidation and selective oxygenation of 5-Hydroxymethylfurfural. *Adv Mater* 2021;33:e2008823. DOI PubMed
32. Hume-Rothery W. Researches on the nature, properties, and conditions of formation of intermetallic compounds, with special reference to certain compounds of tin. *J Inst Met* 1926; 35:295-361.
33. Hume-Rothery W, Mabbott G, W, Channel Evans K. The freezing points, melting points, and solid solubility limits of the alloys of sliver and copper with the elements of the b sub-groups. *Phil Trans R Soc Lond A* 1934;233:1-97. DOI
34. Mizutani U. The hume-rothery rules for structurally complex alloy phases. Surface properties and engineering of complex intermetallics. World scientific; 2010. pp. 323-99. DOI
35. R. The theory of the properties of metals and alloys. *Nature* 1937;139:348-9. DOI
36. Yannello VJ, Fredrickson DC. Generality of the 18-n rule: intermetallic structural chemistry explained through isolobal analogies to transition metal complexes. *Inorg Chem* 2015;54:11385-98. DOI PubMed
37. Fredrickson DC. Parallels in structural chemistry between the molecular and metallic realms revealed by complex intermetallic phases. *Acc Chem Res* 2018;51:248-57. DOI PubMed
38. Nesper R. The Zintl-Klemm concept - a historical survey. *Z anorg allg Chem* 2014;640:2639-48. DOI
39. Schütz M, Gemel C, Klein W, Fischer RA, Fässler TF. Intermetallic phases meet intermetalloid clusters. *Chem Soc Rev* 2021;50:8496-510. DOI PubMed
40. Miller GJ, Schmidt MW, Wang F, You T. Quantitative advances in the Zintl-Klemm formalism. In: Fässler TF, editor. Zintl Phases. Berlin: Springer Berlin Heidelberg; 2011. pp. 1-55. DOI
41. Wang Y, He J, Liu C, Chong WH, Chen H. thermodynamics versus kinetics in nanosynthesis. *Angew Chem Int Ed Engl* 2015;54:2022-51. DOI
42. Xia Y, Xiong Y, Lim B, Skrabalak SE. Shape-controlled synthesis of metal nanocrystals: simple chemistry meets complex physics? *Angew Chem Int Ed Engl* 2009;48:60-103. DOI PubMed PMC
43. Wu J, Yang H. Platinum-based oxygen reduction electrocatalysts. *Acc Chem Res* 2013;46:1848-57. DOI

44. You H, Yang S, Ding B, Yang H. Synthesis of colloidal metal and metal alloy nanoparticles for electrochemical energy applications. *Chem Soc Rev* 2013;42:2880-904. DOI PubMed
45. Alloyeau D, Ricolleau C, Mottet C, et al. Size and shape effects on the order-disorder phase transition in CoPt nanoparticles. *Nat Mater* 2009;8:940-6. DOI PubMed
46. Gibbs J W. The scientific papers of J. Willard Gibbs. *Nature* 1907;75:361-2. DOI
47. Kayser FX, Patterson JW. Sir William Chandler Roberts-Austen - His role in the development of binary diagrams and modern physical metallurgy. *JPE* 1998;19:11-8. DOI
48. Clarke SM, Amsler M, Walsh JPS, et al. Creating binary Cu-Bi compounds via high-pressure synthesis: a combined experimental and theoretical study. *Chem Mater* 2017;29:5276-85. DOI
49. Terayama K, Tamura R, Nose Y, et al. Efficient construction method for phase diagrams using uncertainty sampling. *Phys Rev Materials* 2019:3. DOI
50. Oliynyk AO, Mar A. Discovery of intermetallic compounds from traditional to machine-learning approaches. *Acc Chem Res* 2018;51:59-68. DOI PubMed
51. Kim HY, Joo SH. Recent advances in nanostructured intermetallic electrocatalysts for renewable energy conversion reactions. *J Mater Chem A* 2020;8:8195-217. DOI
52. Avrami M. Kinetics of phase change. I general theory. *J Chem Phys* 1939;7:1103-12. DOI
53. Avrami M. Kinetics of phase change. II transformation-time relations for random distribution of nuclei. *J Chem Phys* 1940;8:212-24. DOI
54. Avrami M. Granulation, phase change, and microstructure kinetics of phase change. III. *J Chem Phys* 1941;9:177-84. DOI
55. Bai J, Yang L, Jin Z, Ge J, Xing W. Advanced Pt-based intermetallic nanocrystals for the oxygen reduction reaction. *Chinese J Catal* 2022;43:1444-58. DOI
56. Zhang J, Zhang L, Cui Z. Strategies to enhance the electrochemical performances of Pt-based intermetallic catalysts. *Chem Commun* 2021;57:11-26. DOI
57. Zhang S, Guo S, Zhu H, Su D, Sun S. Structure-induced enhancement in electrooxidation of trimetallic FePtAu nanoparticles. *J Am Chem Soc* 2012;134:5060-3. DOI
58. Zhang S, Qi W, Huang B. Size effect on order-disorder transition kinetics of FePt nanoparticles. *J Chem Phys* 2014;140:044328. DOI
59. Tzitzios V, Basina G, Gjoka M, et al. The effect of Mn doping in FePt nanoparticles on the magnetic properties of the $L1_0$ phase. *Nanotechnology* 2006;17:4270-3. DOI PubMed
60. Qi W, Li Y, Xiong S, Lee ST. Modeling size and shape effects on the order-disorder phase-transition temperature of CoPt nanoparticles. *Small* 2010;6:1996-9. DOI
61. Oezaslan M, Heggen M, Strasser P. Size-dependent morphology of dealloyed bimetallic catalysts: linking the nano to the macro scale. *J Am Chem Soc* 2012;134:514-24. DOI PubMed
62. Kim SI, Eom G, Kang M, et al. Composition-selective fabrication of ordered intermetallic Au-Cu nanowires and their application to nano-size electrochemical glucose detection. *Nanotechnology* 2015; 26:245702. DOI PubMed
63. Dai ZR, Sun S, Wang ZL. Phase transformation, coalescence, and twinning of monodisperse fept nanocrystals. *Nano Lett* 2001;1:443-7. DOI
64. Supansomboon S, Dowd A, Gentle A, van der Lingen E, Cortie M. Thin films of $PtAl_2$ and $AuAl_2$ by solid-state reactive synthesis. *Thin Solid Films* 2015;589:805-12. DOI
65. Kondoh K, Oginuma H, Kimura A, Matsukawa S, Aizawa T. *In situ* Synthesis of Mg_2Si Intermetallics via powder metallurgy process. *Mater Trans* 2003;44:981-5. DOI
66. Winiarski M, Griveau J, Colineau E, et al. Synthesis and properties of AxV2Al20 (A = Th, U, Np, Pu) ternary actinide aluminides. *J Alloys Compd* 2017; 696:1113-9. DOI
67. Shablinskaya K, Murashova E, Tursina A, Kurenbaeva Z, Yaroslavtsev A, Seropegin Y. Intermetallics $La_9Ru_4In_5$ and $Ce_9Ru_4Ga_5$ with new types of structures. Synthesis, crystal structures, physical properties. *Intermetallics* 2012;23:106-10. DOI
68. Fernandes BB, Ramos ECT, Silva G, Ramos AS. Preparation of Nb-25Si, Nb-37.5Si, Nb-66.6Si powders by high-energy ball milling and subsequent heat treatment. *J Alloys Compd* 2007;434-435:509-13. DOI
69. Alanko GA, Jaques B, Bateman A, Butt DP. Mechanochemical synthesis and spark plasma sintering of the cerium silicides. *J Alloys Compd* 2014;616:306-11. DOI
70. Wang Z, Liu J, Wu X, et al. Engineering ordered vacancies and atomic arrangement over the intermetallic PdM/CNT (M = Pb, Sn, In) nanocatalysts for synergistically promoting electrocatalysis N_2 fixation. *Appl. Catal. B Environ* 2022;314:121465. DOI
71. Abe H, Matsumoto F, Alden LR, Warren SC, Abruña HD, DiSalvo FJ. Electrocatalytic performance of fuel oxidation by Pt_3Ti nanoparticles. *J Am Chem Soc* 2008;130:5452-8. DOI PubMed
72. Chi M, Wang C, Lei Y, et al. Surface faceting and elemental diffusion behaviour at atomic scale for alloy nanoparticles during in situ annealing. *Nat Commun* 2015;6:8925. DOI PubMed PMC
73. Yu W, Zhang Y, Qin Y, et al. High□Density frustrated lewis pair for high-performance hydrogen evolution. *Adv. Energy Mater* 2023;13:2203136. DOI
74. Yoo TY, Yoo JM, Sinha AK, et al. Direct synthesis of intermetallic platinum-alloy nanoparticles highly loaded on carbon supports for efficient electrocatalysis. *J Am Chem Soc* 2020;142:14190-200. DOI PubMed

75. Chen D, Li Z, Zhou Y, et al. Fe_3Pt intermetallic nanoparticles anchored on N-doped mesoporous carbon for the highly efficient oxygen reduction reaction. *Chem Commun* 2020;56:4898-901. DOI
76. Shen T, Gong M, Xiao D, et al. Engineering location and supports of atomically ordered $L1_0$-PdFe intermetallics for ultra-anticorrosion electrocatalysis. *Adv Funct Materials* 2022;32:2203921. DOI
77. Yang CL, Wang LN, Yin P, et al. Sulfur-anchoring synthesis of platinum intermetallic nanoparticle catalysts for fuel cells. *Science* 2021;374:459-64. DOI
78. Ji X, Lee KT, Holden R, et al. Nanocrystalline intermetallics on mesoporous carbon for direct formic acid fuel cell anodes. *Nat Chem* 2010;2:286-93. DOI
79. He W, Zhang X, Zheng K, et al. Structural evolution of anatase-supported platinum nanoclusters into a platinum-titanium intermetallic containing platinum single atoms for enhanced catalytic co oxidation. *Angew Chem Int Ed Engl* 2023;62:e202213365. DOI PubMed
80. Bernal S, Calvino J, Gatica J, Larese C, López-cartes C, Pérez-omil J. Nanostructural evolution of a Pt/CeO_2Catalyst reduced at increasing temperatures (473-1223 k): a hrem study. *J Catal* 1997;169:510-5. DOI
81. Maligal-ganesh RV, Xiao C, Goh TW, et al. A ship-in-a-bottle strategy to synthesize encapsulated intermetallic nanoparticle catalysts: exemplified for furfural hydrogenation. *ACS Catal* 2016;6:1754-63. DOI
82. Takahashi Y, Kadono T, Yamamoto S, et al. Orbital magnetic moment and coercivity of SiO_2 -coated FePt nanoparticles studied by x-ray magnetic circular dichroism. *Phys Rev B* 2014:90. DOI
83. Kim J, Rong C, Liu JP, Sun S. Dispersible ferromagnetic fept nanoparticles. *Adv Mater* 2009;21:906-9. DOI
84. Song TW, Xu C, Sheng ZT, et al. Small molecule-assisted synthesis of carbon supported platinum intermetallic fuel cell catalysts. *Nat Commun* 2022;13:6521. DOI PubMed PMC
85. Chen H, Yu Y, Xin HL, et al. Coalescence in the thermal annealing of nanoparticles: an in situ STEM study of the growth mechanisms of ordered Pt-Fe nanoparticles in a KCL matrix. *Chem Mater* 2013;25:1436-42. DOI
86. Chen H, Wang D, Yu Y, et al. A surfactant-free strategy for synthesizing and processing intermetallic platinum-based nanoparticle catalysts. *J Am Chem Soc* 2012;134:18453-9. DOI
87. Wang Z, Wu X, Liu J, et al. Ordered Vacancies on the body-centered cubic PdCu nanocatalysts. *Nano Lett* 2021;21:9580-6. DOI
88. Meng C, Zhao G, Shi XR, Chen P, Liu Y, Lu Y. Oxygen-deficient metal oxides supported nano-intermetallic $InNi_3C(0.5)$ toward efficient CO_2 hydrogenation to methanol. *Sci Adv* 2021;7:32. DOI PubMed PMC
89. Li Q, Wu L, Wu G, et al. New approach to fully ordered fct-FePt nanoparticles for much enhanced electrocatalysis in acid. *Nano Lett* 2015;15:2468-73. DOI
90. Kim J, Rong C, Lee Y, Liu JP, Sun S. From core/shell structured $FePt/Fe_3O_4$ /MgO to ferromagnetic FePt nanoparticles. *Chem Mater* 2008;20:7242-5. DOI
91. Wang T, Liang J, Zhao Z, et al. Sub-6 nm Fully Ordered $L1_0$-Pt-Ni-Co Nanoparticles enhance oxygen reduction via Co doping induced ferromagnetism enhancement and optimized surface strain. *Adv Energy Mater* 2019;9:1803771. DOI
92. Chen H, Zhang M, Zhang K, et al. Screening and understanding lattice silicon-controlled catalytically active site motifs from a library of transition metal-silicon intermetallics. *Small* 2022;18:e2107371. DOI
93. Chen H, Zou X. Intermetallic borides: structures, synthesis and applications in electrocatalysis. *Inorg Chem Front* 2020;7:2248-64. DOI
94. Guo F, Wu Y, Ai X, et al. A class of metal diboride electrocatalysts synthesized by a molten salt-assisted reaction for the hydrogen evolution reaction. *Chem Commun* 2019;55:8627-30. DOI
95. Li Q, Zou X, Ai X, Chen H, Sun L, Zou X. Revealing activity trends of metal diborides toward pH-universal hydrogen evolution electrocatalysts with Pt-like activity. *Adv Energy Mater* 2018;9:1803369. DOI
96. Ai X, Zou X, Chen H, et al. Transition-Metal-Boron intermetallics with strong interatomic d-sp orbital hybridization for high-performance electrocatalysis. *Angew Chem Int Ed Engl* 2020;59:3961-5. DOI PubMed
97. Yuan Y, Yang Z, Lai W, et al. Intermetallic compounds: liquid-phase synthesis and electrocatalytic applications. *Chemistry* 2021;27:16564-80. DOI PubMed
98. Rong H, Mao J, Xin P, et al. Kinetically controlling surface structure to construct defect-rich intermetallic nanocrystals: effective and stable catalysts. *Adv Mater* 2016;28:2540-6. DOI
99. Liao H, Zhu J, Hou Y. Synthesis and electrocatalytic properties of PtBi nanoplatelets and PdBi nanowires. *Nanoscale* 2014;6:1049-55. DOI PubMed
100. Maksimuk S, Yang S, Peng Z, Yang H. Synthesis and characterization of ordered intermetallic PtPb nanorods. *J Am Chem Soc* 2007;129:8684-5. DOI
101. Cable RE, Schaak RE. Low-Temperature solution synthesis of nanocrystalline binary intermetallic compounds using the polyol process. *Chem Mater* 2005;17:6835-41. DOI
102. Guo J, Jiao S, Ya X, et al. Intermetallic nanocrystals: seed-mediated synthesis and applications in electrocatalytic reduction reactions. *Chemistry* 2022;28:e202202221. DOI
103. Samanta A, Das S, Jana S. Ultra-small intermetallic NiZn nanoparticles: a non-precious metal catalyst for efficient electrocatalysis. *Nanoscale Adv* 2020;2:417-24. DOI PubMed PMC
104. Bu L, Zhang N, Guo S, et al. Biaxially strained PtPb/Pt core/shell nanoplate boosts oxygen reduction catalysis. *Science* 2016;354:1410-4. DOI

105. Chen W, Yu R, Li L, Wang A, Peng Q, Li Y. A seed-based diffusion route to monodisperse intermetallic CuAu nanocrystals. *Angew Chem Int Ed Engl* 2010;49:2917-21. DOI
106. Clarysse J, Moser A, Yarema O, Wood V, Yarema M. Size- and composition-controlled intermetallic nanocrystals via amalgamation seeded growth. *Sci Adv* 2021:7. DOI PubMed PMC
107. Chen H, Liang X, Liu Y, Ai X, Asefa T, Zou X. Active site engineering in porous electrocatalysts. *Adv Mater* 2020;32:e2002435. DOI
108. Zhang M, Zhang K, Ai X, et al. Theory-guided electrocatalyst engineering: From mechanism analysis to structural design. *Chinese J Catal* 2022;43:2987-3018. DOI
109. Seh ZW, Kibsgaard J, Dickens CF, Chorkendorff I, Nørskov JK, Jaramillo TF. Combining theory and experiment in electrocatalysis: insights into materials design. *Science* 2017; 355:eaad4998. DOI PubMed
110. Chatenet M, Pollet BG, Dekel DR, et al. Water electrolysis: from textbook knowledge to the latest scientific strategies and industrial developments. *Chem Soc Rev* 2022;51:4583-762. DOI PubMed PMC
111. Li Z, Qi Z, Wang S, et al. In Situ Formed Pt_3Ti Nanoparticles on a Two-Dimensional Transition Metal Carbide (MXene) used as efficient catalysts for hydrogen evolution reactions. *Nano Lett* 2019;19:5102-8. DOI
112. Hu M, Cai Z, Yang S, et al. Direct growth of uniform bimetallic core-shell or intermetallic nanoparticles on carbon via a surface-confinement strategy for electrochemical hydrogen evolution reaction. *Adv Funct Materials* 2023;33:2212097. DOI
113. Zhao P, Zhang B, Hao X, Yi W, Chen J, Cao Q. Rational design and synthesis of adjustable Pt and Pt-based 3D-nanoframeworks. *ACS Appl Energy Mater* 2022;5:942-50. DOI
114. Lin C, Huang Z, Zhang Z, et al. Structurally ordered Pt_3Co nanoparticles anchored on N-Doped graphene for highly efficient hydrogen evolution reaction. *ACS Sustainable Chem Eng* 2020;8:16938-45. DOI
115. Zhang J, Zhang L, Liu J, et al. OH spectator at IrMo intermetallic narrowing activity gap between alkaline and acidic hydrogen evolution reaction. *Nat Commun* 2022;13:5497. DOI PubMed PMC
116. Zou X, Wang L, Ai X, Chen H, Zou X. Crystal phase-dependent electrocatalytic hydrogen evolution performance of ruthenium-boron intermetallics. *Chem Commun* 2020;56:3061-4. DOI PubMed
117. Chen D, Zhu J, Pu Z, Mu S. Anion modulation of Pt-group metals and electrocatalysis applications. *Chemistry* 2021;27:12257-71. DOI
118. Li Z, Xie Z, Chen H, et al. Realization of interstitial boron ordering and optimal near-surface electronic structure in Pd-B alloy electrocatalysts. *J Chem Eng* 2021;419:129568. DOI
119. Ren Z, Jiang H, Yuan M, et al. Si regulation of hydrogen adsorption on nanoporous PdSi hybrids towards enhancing electrochemical hydrogen evolution activity. *Inorg Chem Front* 2023;10:1101-11. DOI
120. Pu Z, Liu T, Zhang G, et al. General synthesis of Transition-Metal-Based Carbon-Group Intermetallic catalysts for efficient electrocatalytic hydrogen evolution in wide pH range. *Adv. Energy Mater* 2022;12:2200293. DOI
121. Chen D, Pu Z, Wang P, et al. Mapping hydrogen evolution activity trends of intermetallic Pt-group silicides. *ACS Catal* 2022;12:2623-31. DOI
122. Fu L, Li Y, Yao N, Yang F, Cheng G, Luo W. IrMo nanocatalysts for efficient alkaline hydrogen electrocatalysis. *ACS Catal* 2020;10:7322-7. DOI
123. Chen L, Guo X, Shao R, et al. Structurally ordered intermetallic Ir_3V electrocatalysts for alkaline hydrogen evolution reaction. *Nano Energy* 2021;81:105636. DOI
124. Chen H, Ai X, Liu W, et al. Promoting subordinate, efficient ruthenium sites with interstitial silicon for Pt-like electrocatalytic activity. *Angew Chem Int Ed Engl* 2019;58:11409-13. DOI
125. Shen S, Hu Z, Zhang H, et al. Highly active Si sites enabled by negative valent ru for electrocatalytic hydrogen evolution in LaRuSi. *Angew Chem Int Ed Engl* 2022;61:e202206460. DOI PubMed
126. He Y, Wang TL, Zhang M, et al. Discovery and facile synthesis of a new silicon based family as efficient hydrogen evolution reaction catalysts: a computational and experimental investigation of metal monosilicides. *Small* 2021;17:e2006153. DOI
127. Zhang H, Shi P, Ma X, et al. Construction of ordered atomic donor-acceptor architectures in bcc IrGa intermetallic compounds toward highly electroactive and stable overall water splitting. *Adv. Energy Mater* 2023;13:2202703. DOI
128. Wang Y, Lv H, Sun L, Jia F, Liu B. Ordered mesoporous intermetallic trimetals for efficient and pH-Universal hydrogen evolution electrocatalysis. *Adv. Energy Mate* ;12:2201478. DOI
129. Ji SJ, Xue HG, Suen NT. Lanthanide contraction regulates the HER activity of iron triad intermetallics in alkaline media. *Chem Commun* 2020;56:14303-6. DOI PubMed
130. Song R, Han J, Okugawa M, et al. Ultrafine nanoporous intermetallic catalysts by high-temperature liquid metal dealloying for electrochemical hydrogen production. *Nat Commun* 2022;13:5157. DOI PubMed PMC
131. Zhou Q, Hao Q, Li Y, et al. Free-standing trimodal porous NiZn intermetallic and Ni heterojunction as highly efficient hydrogen evolution electrocatalyst in the alkaline electrolyte. *Nano Energy* 2021;89:106402. DOI
132. Li Y, Lu W, Du Y, et al. Co_3W intermetallic compound as an efficient hydrogen evolution electrocatalyst for water splitting and electrocoagulation in non-acidic media. *J Chem Eng* 2022;438:135517. DOI
133. Kibsgaard J, Chorkendorff I. Considerations for the scaling-up of water splitting catalysts. *Nat Energy* 2019;4:430-3. DOI
134. Shao M, Chang Q, Dodelet JP, Chenitz R. Recent advances in electrocatalysts for oxygen reduction reaction. *Chem Rev* 2016;116:3594-657. DOI PubMed

135. Bing Y, Liu H, Zhang L, Ghosh D, Zhang J. Nanostructured Pt-alloy electrocatalysts for PEM fuel cell oxygen reduction reaction. *Chem Soc Rev* 2010;39:2184-202. DOI
136. Lim J, Jung C, Hong D, et al. Atomically ordered Pt_3Mn intermetallic electrocatalysts for the oxygen reduction reaction in fuel cells. *J Mater Chem A* 2022;10:7399-408. DOI
137. Tetteh EB, Gyan-Barimah C, Lee HY, et al. Strained Pt(221) *Facet* in a PtCo@Pt-Rich catalyst boosts oxygen reduction and hydrogen evolution activity. *ACS Appl Mater Interfaces* 2022;14:25246-56. DOI
138. Guan J, Yang S, Liu T, et al. Intermetallic FePt@PtBi core-shell nanoparticles for oxygen reduction electrocatalysis. *Angew Chem Int Ed Engl* 2021;60:21899-904. DOI PubMed
139. Brown R, Vorokhta M, Khalakhan I, et al. Unraveling the surface chemistry and structure in highly active sputtered Pt_3Y Catalyst films for the oxygen reduction reaction. *ACS Appl Mater Interfaces* 2020;12:4454-62. DOI
140. Peera SG, Lee TG, Sahu AK. Pt-rare earth metal alloy/metal oxide catalysts for oxygen reduction and alcohol oxidation reactions: an overview. *Sustain Energy Fuels* 2019;3:1866-91. DOI
141. Zhu S, Yang L, Bai J, et al. Ultra-stable Pt5La intermetallic compound towards highly efficient oxygen reduction reaction. *Nano Res* 2023;16:2035-40. DOI
142. Vej-hansen UG, Escudero-escribano M, Velázquez-palenzuela A, et al. New platinum alloy catalysts for oxygen electroreduction based on alkaline earth metals. *Electrocatalysis* 2017;8:594-604. DOI
143. Stamenkovic VR, Mun BS, Arenz M, et al. Trends in electrocatalysis on extended and nanoscale Pt-bimetallic alloy surfaces. *Nat Mater* 2007;6:241-7. DOI
144. Chen C, Kang Y, Huo Z, et al. Highly crystalline multimetallic nanoframes with three-dimensional electrocatalytic surfaces. *Science* 2014;343:1339-43. DOI PubMed
145. Ding H, Wang P, Su C, et al. Epitaxial growth of ultrathin highly crystalline Pt-Ni nanostructure on a metal carbide template for efficient oxygen reduction reaction. *Adv Mater* 2022;34:e2109188. DOI PubMed
146. Weber P, Weber DJ, Dosche C, Oezaslan M. Highly durable Pt-based core-shell catalysts with metallic and oxidized Co species for boosting the oxygen reduction reaction. *ACS Catal* 2022;12:6394-408. DOI
147. Shi W, Park A, Kwon Y. Scalable synthesis of (Pd,Cu)@Pt core-shell catalyst with high ORR activity and durability. *J Electroanal Chem* 2022;918:116451. DOI
148. Cheng Q, Yang S, Fu C, et al. High-loaded sub-6 nm Pt1Co1 intermetallic compounds with highly efficient performance expression in PEMFCs. *Energy Environ Sci* 2022;15:278-86. DOI
149. Zeng WJ, Wang C, Yan QQ, Yin P, Tong L, Liang HW. Phase diagrams guide synthesis of highly ordered intermetallic electrocatalysts: separating alloying and ordering stages. *Nat Commun* 2022;13:7654. DOI PubMed PMC
150. Wu Z, Shan S, Xie Z, et al. Revealing the role of phase structures of bimetallic nanocatalysts in the oxygen reduction reaction. *ACS Catal* 2018;8:11302-13. DOI
151. Gamler JTL, Shin K, Ashberry HM, et al. Intermetallic Pd_3Pb nanocubes with high selectivity for the 4-electron oxygen reduction reaction pathway. *Nanoscale* 2020;12:2532-41. DOI
152. Feng Y, Shao Q, Ji Y, et al. Surface-modulated palladium-nickel icosahedra as high-performance non-platinum oxygen reduction electrocatalysts. *Sci Adv* 2018;4:eaap8817. DOI PubMed PMC
153. Guo J, Gao L, Tan X, et al. Template-Directed rapid synthesis of Pd-based ultrathin porous intermetallic nanosheets for efficient oxygen reduction. *Angew Chem Int Ed Engl* 2021;60:10942-9. DOI PubMed
154. Cui M, Yang C, Hwang S, et al. Multi-principal elemental intermetallic nanoparticles synthesized via a disorder-to-order transition. *Sci Adv* 2022;8:eabm4322. DOI PubMed PMC
155. Birdja YY, Pérez-gallent E, Figueiredo MC, Göttle AJ, Calle-vallejo F, Koper MTM. Advances and challenges in understanding the electrocatalytic conversion of carbon dioxide to fuels. *Nat Energy* 2019;4:732-45. DOI
156. Ross MB, De Luna P, Li Y, et al. Designing materials for electrochemical carbon dioxide recycling. *Nat Catal* 2019;2:648-58. DOI
157. Gao D, Arán-ais RM, Jeon HS, Roldan Cuenya B. Rational catalyst and electrolyte design for CO_2 electroreduction towards multicarbon products. *Nat Catal* 2019;2:198-210. DOI
158. Nitopi S, Bertheussen E, Scott SB, et al. Progress and perspectives of electrochemical CO_2 reduction on copper in aqueous electrolyte. *Chem Rev* 2019;119:7610-72. DOI
159. Kim C, Dionigi F, Beermann V, Wang X, Möller T, Strasser P. Alloy Nanocatalysts for the electrochemical oxygen reduction (ORR) and the direct electrochemical carbon dioxide reduction reaction (CO_2RR). *Adv Mater* 2019;31:e1805617. DOI PubMed
160. Gamler JTL, Ashberry HM, Skrabalak SE, Koczkur KM. Random alloyed versus intermetallic nanoparticles: a comparison of electrocatalytic performance. *Adv Mater* 2018:e1801563. DOI PubMed
161. Kortlever R, Peters I, Koper S, Koper MTM. Electrochemical CO_2 reduction to formic acid at low overpotential and with high faradaic efficiency on carbon-supported bimetallic Pd-Pt Nanoparticles. *ACS Catal* 2015;5:3916-23. DOI
162. Fan L, Xia C, Zhu P, Lu Y, Wang H. Electrochemical CO_2 reduction to high-concentration pure formic acid solutions in an all-solid-state reactor. *Nat Commun* 2020;11:3633. DOI PubMed PMC
163. He B, Jia L, Cui Y, et al. $SnSe_2$ nanorods on carbon cloth as a highly selective, active, and flexible electrocatalyst for electrochemical reduction of CO_2 into formate. *ACS Appl Energy Mater* 2019;2:7655-62. DOI
164. Yang Q, Zhao Y, Meng L, et al. Nanoporous intermetallic snte enables efficient electrochemical CO_2 reduction into formate via promoting the fracture of metal-oxygen bonding. *Small* 2022;18:e2107968. DOI

165. Wan WB, Zhou YT, Zeng SP, et al. Nanoporous intermetallic Cu_3Sn/Cu Hybrid electrodes as efficient electrocatalysts for carbon dioxide reduction. *Small* 2021;17:e2100683. DOI PubMed
166. Kim D, Xie C, Becknell N, et al. Electrochemical activation of CO_2 through atomic ordering transformations of AuCu nanoparticles. *J Am Chem Soc* 2017;139:8329-36. DOI PubMed
167. Jia L, Sun M, Xu J, et al. Phase-Dependent electrocatalytic CO_2 reduction on Pd_3Bi nanocrystals. *Angew Chem Int Ed Engl* 2021;60:21741-5. DOI PubMed
168. Bagchi D, Raj J, Singh AK, et al. Structure-Tailored surface oxide on Cu-Ga intermetallics enhances CO_2 reduction selectivity to methanol at ultralow potential. *Adv Mater* 2022;34:e2109426. DOI PubMed
169. Liu D, Chen M, Du X, et al. Development of electrocatalysts for efficient nitrogen reduction reaction under ambient condition. *Adv Funct Mater* 2021;31:2008983. DOI
170. Chen X, Guo Y, Du X, et al. Atomic structure modification for electrochemical nitrogen reduction to ammonia. *Adv Energy Mater* 2020;10:1903172. DOI
171. Montoya JH, Tsai C, Vojvodic A, Nørskov JK. The Challenge of electrochemical ammonia synthesis: a new perspective on the role of nitrogen scaling relations. *ChemSusChem* 2015;8:2180-6. DOI PubMed
172. Zhao J, Chen Z. Single mo atom supported on defective boron nitride monolayer as an efficient electrocatalyst for nitrogen fixation: a computational study. *J Am Chem Soc* 2017;139:12480-7. DOI
173. Abghoui Y, Garden AL, Hlynsson VF, Björgvinsdóttir S, Ólafsdóttir H, Skúlason E. Enabling electrochemical reduction of nitrogen to ammonia at ambient conditions through rational catalyst design. *Phys Chem Chem Phys* 2015;17:4909-18. DOI PubMed
174. Zhou J, Chen X, Guo M, Hu W, Huang B, Yuan D. Enhanced catalytic activity of bimetallic ordered catalysts for nitrogen reduction reaction by perturbation of scaling relations. *ACS Catal* 2023;13:2190-201. DOI
175. Liu X, Jiao Y, Zheng Y, Qiao S. Isolated boron sites for electroreduction of dinitrogen to ammonia. *ACS Catal* 2020;10:1847-54. DOI
176. Ai X, Chen H, Liang X, et al. Metal-coordinating single-boron sites confined in antiperovskite borides for N_2-to-NH_3 catalytic conversion. *ACS Catal* 2022;12:2967-78. DOI
177. Guo J, Wang H, Xue F, et al. Tunable synthesis of multiply twinned intermetallic Pd_3Pb nanowire networks toward efficient N_2 to NH_3 conversion. *J Mater Chem A* 2019;7:20247-53. DOI
178. Tong W, Huang B, Wang P, Shao Q, Huang X. Exposed facet-controlled N_2 electroreduction on distinct Pt_3Fe nanostructures of nanocubes, nanorods and nanowires. *Natl Sci Rev* 2021;8:nwaa088. DOI
179. Chu K, Gu W, Li Q, Liu Y, Tian Y, Liu W. Amorphization activated FeB_2 porous nanosheets enable efficient electrocatalytic N_2 fixation. *J Energy Chem* 2021;53:82-9. DOI
180. Wang X, Luo M, Lan J, Peng M, Tan Y. Nanoporous intermetallic Pd_3 Bi for efficient electrochemical nitrogen reduction. *Adv Mater* 2021;33:e2007733. DOI PubMed
181. Wang T, Liu Q, Li T, et al. A magnetron sputtered Mo_3Si thin film: an efficient electrocatalyst for N_2 reduction under ambient conditions. *J Mater Chem A* 2021;9:884-8. DOI
182. Li X, Zhao J, Su D. Structural Changes of intermetallic catalysts under reaction conditions. *Small Structures* 2021;2:2100011. DOI
183. Li Z, Zhao L, Chen H, et al. Crystal phase-selective synthesis of intermetallic palladium borides and their phase-regulated (electro)catalytic properties. *Catal Sci Technol* 2022;12:1038-42. DOI
184. Wei GF, Zhang LR, Liu ZP. Group-VIII transition metal boride as promising hydrogen evolution reaction catalysts. *Phys Chem Chem Phys* 2018;20:27752-7. DOI PubMed